University of São Paulo–USP
Polytechnic School

Pablo Daniel Paz Salazar

Voltage Stability of Power Grids in the Presence of Increasing Wind Power Penetration

São Paulo

2022

Pablo Daniel Paz Salazar

Voltage Stability of Power Grids in the Presence of Increasing Wind Power Penetration

Versão Corrigida

A thesis presented to the University of Sao Paulo to obtain the title of Doctor of Philosophy

Field: Power Systems

Supervisor: Prof. Dr. Mauricio Barbosa de Camargo Salles
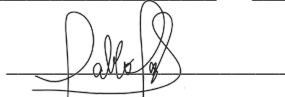Co-supervisor: Prof. Dr. Eduardo Coelho Marques da Costa

São Paulo

2022

Este exemplar foi revisado e corrigido em relação à versão original, sob responsabilidade única do autor e com a anuência de seu orientador.

São Paulo, _21__ de _Novembro_____ de _2022_____

Assinatura do autor: _____

Assinatura do orientador: _Mauricio Salles____

Catalogação-na-publicação

Acknowledgements

Resumo

Paz S, Pablo **Estabilidade de Tensão de Sistemas de Energia na Presença da Crescente Penetração de Energia Eólica**. 73 p. A thesis – Escola Politécnica, Universidade de São Paulo, 2022.

Nas pesquisas desenvolvidas e apresentadas nesta tese, foram feitas contribuições para o estado da arte na área de estabilidade de tensão. A primeira contribuição está relacionada à estabilidade de tensão de longa duração. Uma nova solução analítica foi proposta para encontrar o ponto de bifurcação de sistemas de potência (nariz da curva PV). A solução não está relacionada aos métodos de Newton e pode ser aplicada aos novos desafios das redes elétricas com alta penetração de fontes renováveis. O método proposto é baseado na teoria do cálculo variacional e pode rastrear a bifurcação usando o "último ponto computado", tornando-o adequado para aplicações em tempo real. A segunda parte da tese é dedicada à estabilidade transitória, propondo um novo controle de tensão para um parque eólico. O objetivo é introduzir uma condição de operação "preventiva"capaz de melhorar o tempo crítico de falta durante a ocorrência de um curto circuito. Complementarmente ao controle preventivo, é proposto um controle corretivo local baseado em dados para restaurar rapidamente a tensão de acordo com os requisitos dos *grid codes* modernos. Os dados do *Model Predictive Control* treinam os controladores baseado em dados por meio de uma técnica de aprendizado com consciência de risco. O controle local baseado em dados atualiza as entradas para os controladores PI do compensador síncrono estático e dos geradores eólicos para restaurar a tensão de forma mais eficaz. Os resultados indicam que os controles propostos apresentam melhor desempenho comparando com aqueles baseados na reserva de potência reativa dinâmica.

Palavras-chave: Margem da Estabilidade de Tensão; Controle baseado em dados; Parque Eólico; Modelo de Controle Preditivo.

Abstract

Paz S, Pablo **Voltage Stability of Power Grids in the Presence of Increasing Wind Power Penetration**. 73 p. Ph.D. Thesis – Polytechnic School, University of São Paulo, 2022.

The research carried out and presented in this thesis was performed to contribute to the state-of-the-art in the area of voltage stability. The first contribution is related to long-term voltage stability. A new analytical solution was proposed to find the power system's bifurcation point (the PV curve's nose). The solution is not related to Newton's methods and can be applied to the new challenges of the power grid with high penetration of renewable sources. The proposed method is based on variational calculus theory and can track the bifurcation using the "last computed point,"making it suitable for real-time applications. The second part of the thesis is dedicated to transitory stability, proposing a new voltage control for a wind farm. The objective is to introduce a "preventive"operating condition capable of increasing the critical clearing time during the occurrence of a fault. Complementary to the preventive control, a local data-driven corrective control is proposed to quickly restore the voltage according to the requirements of modern grid codes. Model Predictive Control data train the data-driven controllers through a risk-aware learning technique. The local data-driven control updates the inputs for the PI controllers of the static synchronous compensator and the wind generators to restore voltage more effectively. The results indicate that the proposed controls perform better than those based on the dynamic reactive power reserve.

Keywords: Voltage Stability Margin;Data-Driven Control; Wind Farms; Model Predictive Control.

List of Figures

List of Tables

List of Acronyms

CPF Continuation Power Flow

CVaR Conditional Value at Risk

CSC Convertible Static Compensator

DRPR Dynamic Reactive Power Reserve

DFIG Double-Fed Induction Generator

EFM Extended Functional Method

ESS Energy Storage System

HB Hopf Bifurcation

HV High Voltage

LIB Limited Induced Bifurcation

LVRT Low Voltage Ride Through

ML Machine Learning

MSE Mean Squared Error

MPC Model Predictive Control

MIMO Multi Input Multi Output

MV Medium Voltage

NN Neural Network

OC Operation Condition

ODE *Ordinary Differential Equation*

OPF Optimal Power Flow

PMU *Phasor Measurements Units*

PCC Point of Common Coupling

PI Proportional Integral

PID Proportional Integral Derivative

PML Point of Maximum Loadability

PoC Point of Collapse

PVL Point of Voltage Collapse

QDSA Quasi-Direction of the Steepest Ascent

SNB Saddle-Node Bifurcation

SCADA Supervisory Control and Data Acquisition

STATCOM Static Synchronous Compensator

SVC Static Var Compensator

SVG Static Var Generator

VSM Voltage Stability Margin

VC Voltage Collapse

WF Wind Farm

WG Wind Generator

Contents

CHAPTER **1**

Introduction

In 2019 global carbon dioxide emissions were held at 33 gigatons after two years of growth (IEA, 2019). This stop in carbon emissions can be attributed to the decline in fossil fuel-based energy use in the electricity sector in advanced economies, which have expanded generation based on renewable energies (mainly wind and solar), and high nuclear generation. Since fossil fuels are a finite energy source likely to end in the medium term, besides the need for climate change mitigation, renewable sources, and energy storage systems are the agreed path to replace conventional fossil fuel-based generation. Energy Storage Systems (ESS) are a promising alternative to solve the problem of source intermittency and are currently an area of much research for achieving future operations with 100% renewable (KROPOSKI, 2017).

Due to the climate change mitigation plan, the system's complexity has been rising regarding high meshed networks, high penetration of renewables, and high Flexible AC Transmission System (FACTS) employment, among others. Due to the network's complexity, many possible operating states and uncertainties make system security monitoring a crucial task. Besides, we are facing the new inverter-based microgrid era with many challenges. The main feature of renewable generation is the intermittent nature of the driving force, which causes most challenges regarding new grids. Recently, IEEE Task Forces have described global guidelines challenges for renewable expansion, pointing out voltage control and the real-time voltage stability margin among important challenges to overcome (SUN et al., 2019).

We are living at an inflection point regarding power grid technology. As a result of pursuing decarbonization to mitigate climate change, renewable resource penetration has grown drastically in the last decade in two ways: as conventional power plants injecting power via transmission lines and as distributed resources in distribution grids. Those renewable sources rely on power electronics converters to produce the sinusoidal behavior of conventional synchronous generators. Inverted-based resources are becoming predominant in the power grid and are switching from "grid following" to "grid forming". In this context, academia is making a great effort to draw the power grid of the future, facing

complex challenges such as closing the gap of variable sources feeding a quasi-steady state load, feasible storage systems, and flexible loads, among others.

Voltage stability is a subject of much research and interest because it represents one of the significant threats to the security of power systems. The loss of voltage stability has been the cause of blackouts in North America, Brazil, Europe, and Asia. In the past, voltage instability was associated with weak systems and long lines. Classical techniques to find the exact bifurcation point are unsuitable for real-time application since those techniques are time-consuming and computationally expensive. To surveil the Voltage Stability Margin (VSM), the researchers have developed a wide range of techniques for calculating the VSM, like Thevenin's theorem-based method, PMU-based index, and Artificial Intelligence-based methods, among others. Despite the good performance of those techniques, more accuracy may be needed for scenarios that get away from situations where those techniques work well. For instance, it is not guaranteed that all possible operational conditions in the grid to be generalized by a machine learning training data set.

This thesis makes contributions related to long and short-term voltage stability. Regarding long-term voltage stability, the first part of this work aims to contribute to an often overlooked problem: long-term voltage stability. In the past, voltage stability margin was a concern from a load growth "uncertainty"perspective since conventional generation availability was less uncertain. Nowadays, source generation is becoming more intermittent, and the available methods to calculate the bifurcation point in a "real-time"fashion under this new scenario can be computationally expensive. There are two closed-form solutions to address the bifurcation point that has not been updated since the '90s: the Continuation Power Flow (CPF) and the Point of Collapse (PoC). The CPF is the most popular method to calculate the bifurcation point and is the only technique used in today's most famous power system commercial software. However, as stated before, this method may not be suitable for real-time, which might be imperative for future power systems since CPF's main "path following"feature makes generation variability behavior hard to model. The PoC is another closed-form method characterized by a direct "one point"calculation. However, rely on a robust close guess point solution to start the iteration, which is very difficult to obtain, and that is why it is not included in most popular power system solvers.

This thesis contributes to developing an original method based on the variational theory that can chase the bifurcation point displaced by a change in the network using the initial bifurcation point previous to the change. This "chasing"feature makes the methodology attractive, especially for new power grids constantly subject to topology and generation changes.

The contribution of short-term voltage stability is the development of voltage control of a wind farm which helps to avoid voltage instability during grid faults and enhance LVRT capabilities. A loss minimization preventive control is proposed for the voltage

control of a wind farm. This preventive control can improve critical clearing times and voltage restoration after a fault. Also, a local data-driven corrective control is proposed to enhance the voltage restoration after clearing a fault. The novelty of the data-driven corrective control approach is the application of an innovative way to learn. A "risk-aware learning' technique is used to train a neural network reducing the risk of predictions that could harm the control performance.

1.1 Research Objectives

Since renewable energy technology is constantly improving and considering that further renewable penetration is coming, there is a need to update power system analysis adapted to the intrinsic characteristics of these new technologies. In this context, this work aims to contribute to adapting voltage stability assessment to upcoming power grids characterized by a high renewable source penetration.

The specific objectives are:

❑ Develop a new method to find the bifurcation point of "new grids,"specially adapted to track/chase the bifurcation point displaced by a shift in generation/topology.

❑ Develop a control to improve the short-term voltage stability of a wind farm

1.2 Thesis Structure

In Chapter 2, a brief review of bifurcation theory is presented as a base tool for developing the proposed method to assess voltage stability. Chapter 3 introduces the base of variational calculus and the development to use it for saddle-node bifurcation point calculation. Chapter 4 introduces a loss minimization-based preventive control that improves critical clearing time and voltage restoration. Also, a local data-driven voltage control to restore the voltage after a fault is presented. Chapter 5 presents a conclusion about the results and the upcoming work.

CHAPTER **2**

Long Term Voltage Stability and Bifurcation Theory

The physical model of power systems is usually represented by variables and parameters governed by physics laws and expressed by a set of autonomous ordinary differential equations (ODEs) describing a nonlinear dynamic system. Bifurcations are an intrinsic quality of a nonlinear system related to the qualitative and abrupt change of the system behavior by changing one or more parameters.

In the 1980s, static bifurcation was associated with loss of steady-state stability and voltage collapse in power systems by (ARAPOSTHATIS; SASTRY; VARAIYA, 1981; KWATNY; PASRIJA; BAHAR, 1986). Later on, in the early 1990s, a more in-depth theory on static and dynamic bifurcations was developed for the analysis of voltage stability (DOBSON; CHIANG, 1989; CHIANG et al., 1990; AJJARAPU; LEE, 1992; CANIZARES, 1995). At that time, researchers realized that most events associated with voltage collapse were happening with heavily loaded systems as long-term phenomena.

This way, various voltage stability problems were well adapted from a static perspective, considering a single parameter responsible for the lack of reactive power supply and the voltage drop: the load.

By the static approach, the equilibrium points of the ODEs are represented by a nonlinear system of algebraic equations (e.g., the *power flow*, that are used in the parametric representation to find the bifurcation. The parameter used to find the bifurcation point in the power flow case is the load, and the value of this parameter at the bifurcation point represents the maximum loading capacity.

A voltage stability theory and its relation with bifurcations are presented in this chapter.

2.1   Preliminaries

Consider the following nonlinear dynamic system described by an autonomous differential equation:

$$\dot{x} = f(x, \lambda), x \in \mathbb{R}^n; \lambda \in \mathbb{R}^k \tag{1}$$

Where x denotes the vector of state variables (bus voltage magnitudes, generators angles, generator angular velocities, etc) and the conditions of existence and uniqueness of solution are assumed to be satisfied for $f : \mathbb{R}^n \to \mathbb{R}^n$. λ is a vector of time invariant scalar parameters. A point (x_0, λ_0) is called an *equilibrium point* of (1) if $f(x_0, \lambda_0) = 0$.

The behavior of the system can be explained by two theories which complements each other:

❏ The Hartman-Grobman theorem

   If the Jacobian $\partial f / \partial x_0$ has no eigenvalues with zero real part, then (x_0, λ_0) is an hyperbolic fix point and has the same topological structure than a locally linearized system in (x_0, λ_0). That means that when the eigenvalues has non-zero real part, a linear stability analysis suffices at all.

❏ The Center Manifold Theory

   The points where at least one eigenvalue has zero real part are non-hyperbolic fixed points (x_c, λ_c) and are called Bifurcation points. The bifurcation points are structurally unstable and several branches coalesces at (x_c, λ_c). Here is not possible to use linear stability and the center manifold theory is applied as follows:

   Let (x_0, λ_0) be the equilibrium point of $f(x, \lambda)$. The real part of the eigenvalues (μ) defines the corresponding generalized eigenspaces E^s, E^u, and E^c of the Jacobian matrix $\partial f / \partial x |x_0$ following the next scheme:

$$+Re(\mu) = \begin{cases} < 0 - E^s \\ = 0 - E^c \\ > 0 - E^u \end{cases} \tag{2}$$

   Then the stable W^s, unstable W^u and center manifold W^c are tangential to W^s, W^u and W^c respectively at (x_0, λ_0). The center manifold theory is based on the reduction of the dynamics produced by the flow on the center manifold. Considering that unstable manifold W^u is empty, the nonlinear vector field can be transformed to the following form, in order to calculate the flow of the reduced dynamics on W^c.

$$\dot{x}_c = A_c x_c + f(x_c, x_s); X_c \in \mathbb{R}^n c \tag{3}$$

$$\dot{x}_s = A_s x_s + g(x_c, x_s); X_s \in \mathbb{R}^n s \tag{4}$$

The matrix $A_c(n_c, n_c)$ contains n_c eigenvalues with zero real parts as well as the matrix $A_s(n_s, n_s)$ contains n_s eigenvalues with negative real parts. Due to nonlinear couplings between x_s and x_c, $x_s = h(x_c)$ has to be introduced in (3) to compute the so called **Center Manifold Reduction**, yielding:

$$\dot{x}_c = A_c x_c + f(x_c, h(x_c)); X_c \in \mathbb{R}^n c \tag{5}$$

The center manifold theory states that dynamics of 1 and 5 are equivalent with λ fixed at the value λ.

2.2 Bifurcations

In summary, if x is non-hyperbolic, the local stability behavior is entirely governed by the flow on the center manifold. Centers manifolds play an essential role in bifurcation theory. The center manifold reduction, in combination with some system parameter λ, leads to the concept of bifurcations. The name "bifurcation" was first introduced by Henri Poincaré in 1885 in his first paper in mathematics showing such behavior. Bifurcation is the phenomenon that occurs when a small smooth change made to one or more parameter values of a system causes a sudden 'qualitative' or topological change in its behavior. The number of possible types of bifurcation increases rapidly with an increasing dimension of the parameter space. The bifurcations are organized hierarchically with increasing co-dimension, where co-dimension is the lowest dimension of a parameter space necessary to observe a given bifurcation phenomenon. From here onward, we will discuss only the dynamical system with a single parameter variation.

Changing this parameter may drive the system into a critical state at which the eigenvalues will define the bifurcation type according to the following values:

❑ Static Bifurcation A real eigenvalue becomes zero, and new branches of stationary solutions usually arise and are called static. Typical static bifurcations are saddle-node, trans-critical, pitchfork, and limited induced.

❑ Dynamic Bifurcation A pair of complex conjugate eigenvalues become imaginary and may lead to the birth of a branch of periodic solutions. Typical dynamical bifurcation is Hopf.

The bifurcations mentioned above are local types. Global bifurcation will be no treated in this work.

2.3 Detection of Bifurcation Points in Power Systems

In this work, only common bifurcation in power systems will be shown, like Saddle Node Bifurcation (SNB), Limited Induced Bifurcation (LIB), and Hopf Bifurcation (HB).

Before going into detail about each type of bifurcation, some definitions used in power systems are explained.

2.3.1   Voltage stability definition

The IEEE/CIGRE Joint Task Force on Stability Terms and Definitions defines voltage sytability as follows: *Voltage stability refers to the ability of a power system to maintain steady voltages at all buses in the system after being subjected to a disturbance from a given initial operating condition* (KUNDUR et al., 2004). Voltage stability can be divided into long and short-term voltage stability. Long-term voltage stability is generally related to loading change, and short-term voltage stability is related to disturbances.

2.3.2   Voltage Collapse (VC) and Point of Voltage Collapse (PVC)

Voltage Collapse (VC) happens when the system stability is lost due to the birth of any bifurcation. The Point of Voltage Collapse (PVC) is the value of all the variables of the EDO at which the Voltage Collapse happens, being the load parameter of particular interest. The PVC load represents the power system's maximum loading condition. The PVC is often called The Point Of Maximum Loadability (PML).

2.3.3   Voltage Stability Margin (VSM)

The Voltage Stability Margin is the difference between the value of the load at the PVC and the current load. It represents how much load can be increased in the power system until the PVC.

2.4   Saddle Node Bifurcations (SNB)

In the '80s, a major discussion was if the VC was a static or dynamic event. Both kinds of events were successfully approached and are helpful depending on the scenario. Given the longer time frame involved and supposing the load parameter varies slowly with time, researchers agree that for the calculation of the VSM, the static analysis is a suitable approach and can give a reasonable accuracy. The advantage of the static approach is that it is computationally much more straightforward than the dynamic approach. The saddle-node bifurcation consists of the stable equilibrium x_0 coalescing with a nearby unstable type one equilibrium x_1 and disappearing, causing the system to lose stability (DOBSON, 1992).

The Jacobian $\partial f(x_*, \lambda_*)/\partial x$ is singular and has a unique simple zero eigenvalue with a corresponding right eigenvector v_* so that $(\partial f(x_*, \lambda_*)/\partial x)v_* = 0$. Where x_* and λ_* are

the critical values for the state vector (bus voltage magnitudes and angles), and the load parameter, respectively.

The model described in (SEYDEL, 1988) states for the equations of equilibria with constraints ensuring a zero eigenvalue at the point of interest. The conditions are expressed as follows:

$$
\begin{cases}
f(x, \lambda) = 0 \\
\left[\dfrac{\partial f(x, \lambda)}{\partial x} \right] v = 0 \\
v \neq 0
\end{cases}
\tag{6}
$$

This method was applied to voltage stability in (ALVARADO, 1989; CANIZARES et al., 1992) and usually is called the Point of Collapse Method (PoC).

In order to point out the SNB and points of equilibria graphically, to follow, the famous PV curve is introduced.

2.4.1 PV Curve

Consider the two bus system in Fig. 1. The Power flow yields Two Voltages at Bus 2 for each load level until it reaches the PML or PVC where the two solutions coalesce in only one point. These two solutions are the stable and unstable equilibrium points. The stable and unstable equilibrium points are in the upper and the lower part of Fig. 2 respectively.

The PV curve is one of the most used methods of voltage stability analysis. The PV curve presents the current Equilibrium Point and the distance to the PVC called VSM. For large meshed networks, P can be the total active load in the load area, and V can be the voltage of the critical or representative bus.

Figure 1 – Two bus system
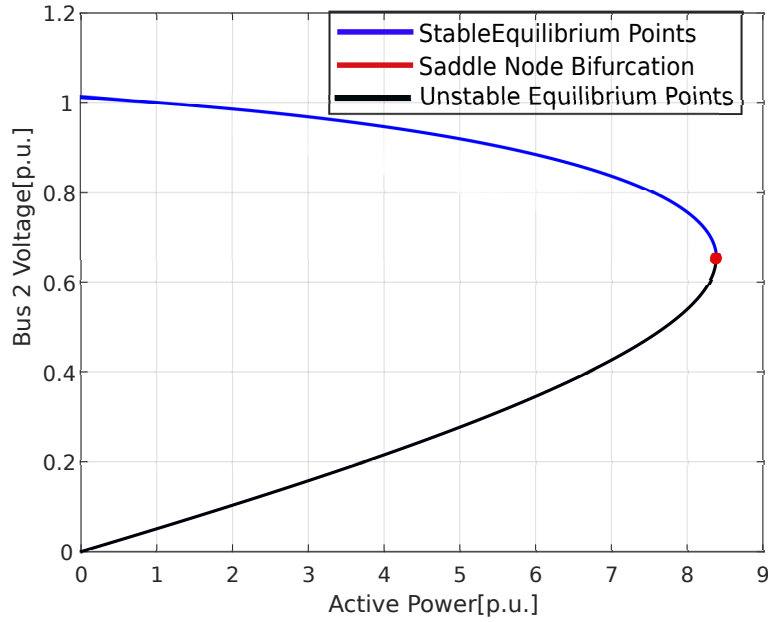
Figure 2 – PV Curve

2.5   Limited Induced Bifurcations (LIB)

After reaching the generator's reactive power limit, the power system becomes more vulnerable. This effect immediately changes the system equations. *Limited Induced Bifurcations* is the phenomenon in which the power systems become immediately unstable when the reactive power limit is reached. This system's instability led the system to VC (DOBSON; LU, 1992).

Consider a general power system modeled by the parametric differential equations $\dot{x} = f(x, \lambda)$, where $x \in \mathbb{R}^n$. When the system is operating at the stable equilibrium point $f(x_0, \lambda_0) = 0$ and the reactive limit is reached, the system equations immediately change to $\dot{x} = f^{lim}(x, \lambda)$ remaining the position x_0. That means $f(x_0, \lambda_0) = f_{lim}(x_0, \lambda_0)$.

There are two possibilities for this encounter; the curves can cross in the stable or unstable parts, as shown in Figures 3 and 4, respectively. In (YUE; VENKATASUBRAMANIAN, 2007), the authors presented the following method to detect the occurrence of LIB. Consider the system around the critical point:

$$\begin{cases} F(x, Q, V, \lambda) = 0 \\ Q < Q_{max} \\ V < V_{ref} \\ (Q - Q_{max})(V - V_{ref}) = 0 \end{cases} \tag{7}$$
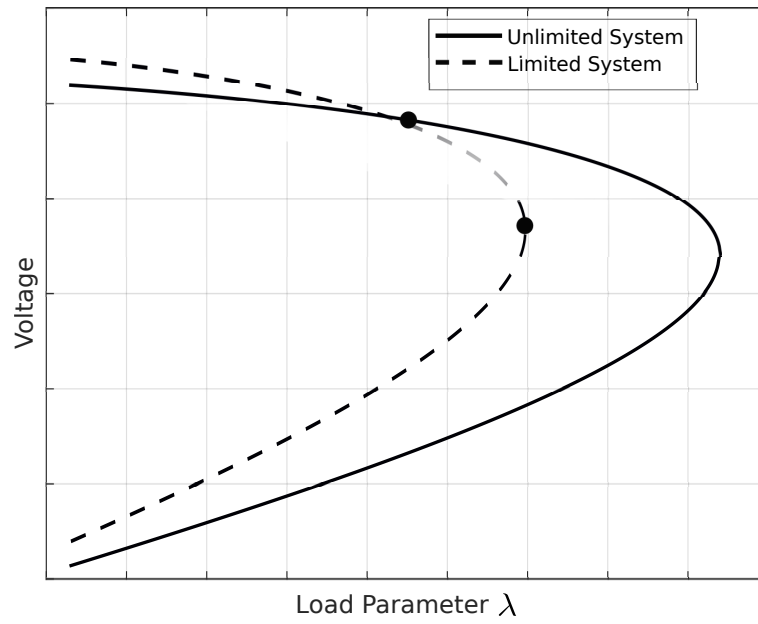
Figure 3 – Limit reached with less VSM
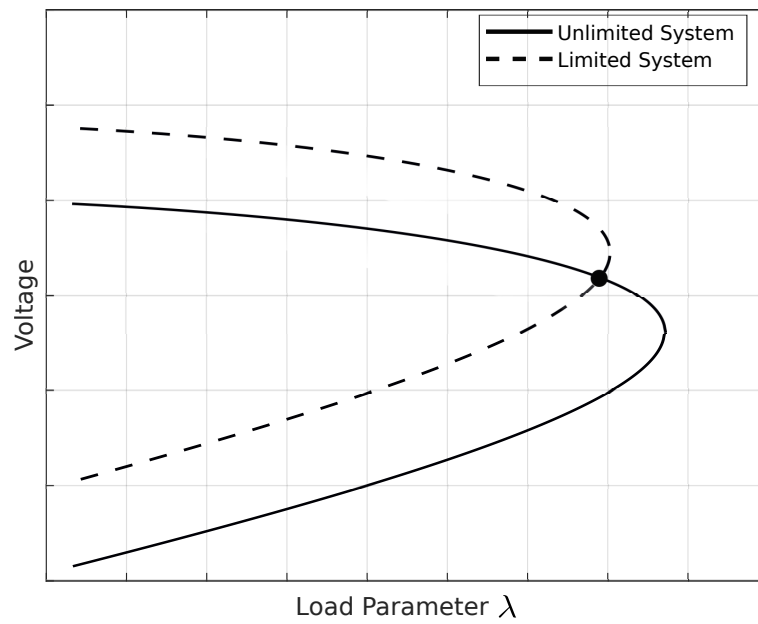
Figure 4 – Immediate instability when limit is reached

Transforming,

$$
\begin{cases}
Q' = h(Q - Q_{max}) \\
V' = h(V - V_{ref})
\end{cases}
\tag{8}
$$

Combining (8) and (9),

$$\begin{cases} F'(x, Q', V', \lambda) = 0 \\ F'(x, Q' + Q_{max}, V' + V_{ref}, \lambda) = 0 \\ Q'V' = 0 \end{cases} \qquad (9)$$

Developing linear algebra, differentiating, and linearizing yields the so-called *Complementary Induced Bifurcation Theorem*:

$$det \left[\frac{\partial \mathbf{F}}{\partial x} \cdot \frac{\partial \mathbf{F}}{\partial Q'} \right] \cdot det \left[\frac{\partial \mathbf{F}}{\partial x} \cdot \frac{\partial \mathbf{F}}{\partial V'} \right] > 0 \qquad (10)$$

2.6   Hopf Bifurcations (HB)

The Hopf Bifurcation is a dynamical bifurcation. Can be detected when a complex conjugate pair of eigenvalues of the Jacobian $\partial f(x, \lambda)/\partial x$ crosses the imaginary axis and moves into the right half-plane (AJJARAPU; LEE, 1992). The system may start oscillating with a small amplitude.

The onset of this oscillatory phenomenon is described by Hopf's Bifurcation theory as follows:

Consider the system $F(x_h, \lambda_h) = 0$. Suppose the Jacobian matrix $[\partial F/\partial x]$ has a simple pair of purely imaginary eigenvalues $u(\lambda_h) = \pm i\omega_0$ (1st Condition) and the derivative $d(Re(u(\lambda_h)))/d\lambda \neq 0$ (2nd Condition). In that case, depending on the second condition's sign, there is a birth or death of limit cycles at (x_h, λ_h). The Hopf bifurcation concludes specifically that a one-parameter family of periodic solutions $x(t, \epsilon)$ always exists in the neighborhood of (x_h, λ_h). If the sign of the second condition is positive, the parameter ϵ can be chosen as follows:

$$x = x_h + \epsilon x_1(t) + ... \qquad (11)$$

$$\lambda = \lambda_h + \lambda_2 \epsilon^2 + ... \qquad (12)$$

$$T = 2\pi/\omega_0 + T_2 \epsilon^2 + ... \qquad (13)$$

The bifurcations discussed so far are the most common in Power Systems. Figure 5 shows the list of possible bifurcations.
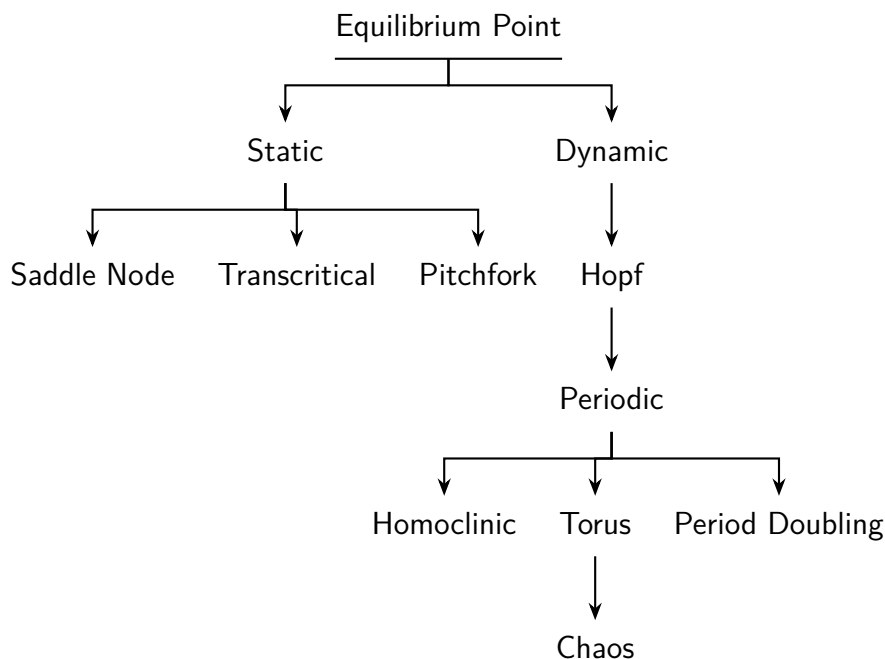
Figure 5 – List of possible bifurcations

2.7 Literature review

To date, there still is research interest in real-time applications to find a suitable tool to predict the collapse point accurately. (VU et al., 1999; BAO; HUANG; XU, 2003; ZHOU; ANNAKKAGE; RAJAPAKSE, 2010; LEONARDI; AJJARAPU, 2010; WANG et al., 2011; LEONARDI; AJJARAPU, 2012; HU et al., 2015; GUTIÉRREZ; RAMIREZ et al., 2014; CHANDRA; PRADHAN, 2019) and to improve short term voltage stability (HAN et al., 2017; HAN; CHEN; MA, 2018).

In this way, a great variety of voltage stability problems were well modeled and analyzed from a static perspective taking into account a single slowly varying parameter: the load. In the static approach, the Power System is represented by a set of nonlinear algebraic equations (the *power flow* equations), and the maximum loading capacity is associated with a bifurcation of these equations as a consequence of load variation.

Several computational techniques were developed from a static perspective to predict the loadability limit in power systems. These techniques can be classified into two categories: indirect or path-following methods and direct methods. For example, the continuation power flow methods (CPF) (AJJARAPU; CHRISTY, 1992; CHIANG et al., 1995) are indirect methods that are widely applied to determine the relationship between power demand and voltage profile (P-V curve). These methods compute the bifurcation point by increasing the load until reaching the loadability limit. On the other hand, direct methods attempt to compute the bifurcation point without computing the system's trajectory from the initial load to the maximum one.

The *Point of Collapse* (PoC) is a direct method used to compute the SNB point solving a set of nonlinear algebraic equations. A closed initial guess of the SNB point is required to ensure convergence. (ALVARADO, 1989; AJJARAPU, 1991; CANIZARES; ALVARADO, 1993; DOBSON; LU, 1993).

In (CANIZARES, 1998b; CANIZARES, 1998a), the calculation of SNBs was formulated in the context of Optimal Power Flow (OPF). In contrast, in (VOURNAS; KARYSTIANOS; MARATOS, 2000; ROSEHART; ROMAN; SCHELLENBERG, 2005), a constrained OPF to calculate the maximum loadability of the system, taking into account the limitation of reactive power generation, was formulated. In (AVALOS et al., 2008), was demonstrated the equivalence between CPF and OPF to calculate SNBs and Limited Induced Bifurcations (LIB).

Recently, novel algorithms with improved computational times have been developed. In (GÓMEZ-QUILES; GÓMEZ-EXPÓSITO; VARGAS, 2015), for instance, the maximum loadability is computed via factored power flow, whereas reference (NEVES; ALBERTO; CHIANG, 2020), presents a fast method for finding LIBs.

Developed Method for Calculating the SNB

This chapter aims to develop a method to monitor the VSM in real time, considering the new characteristics of power grids that imply high penetration of renewable sources. We present the so-called *extended functional method:sub-gradient approach* (IL'YASOV, 2007) as a tool from variational theory and nonsmooth optimization.

3.1 Background on the Extended Functional Method

The main objective of this section is to present a background on the extended functional method introduced in (IL'YASOV, 2007). This method will form the computational basis for further analysis in this thesis.

Consider the power system balance in the following form:

$$f(x, \lambda) = g(x) - \lambda b = 0, \quad x \in Q \subseteq \mathbb{R}^n, \ \lambda \in \mathbb{R}. \tag{f}$$

Here $g : Q \to \mathbb{R}^n$ is continuously differentiable function, Q is an open domain in $\mathbb{R}^n$, $b \in \mathbb{R}^n$, and λ the parameter of load. Hereafter, $\| \cdot \|$, $\langle \cdot, \cdot \rangle$ stand for the Euclidean norm and the scalar product in $\mathbb{R}^n$, respectively; $e_1 = (1, \ldots, 0), \ldots, e_n = (0, \ldots, 1)$ is an orthonormal system of vectors, $\nabla_x := (\partial/\partial x_1 \ldots \partial/\partial x_n)^T$. Throughout the thesis we assume that $b_i > 0$, for all $i \in \{1, \ldots n\}$. Obviously, one can always achieve this condition by multiplying on (-1) and summing equations in (f). In paper (IL'YASOV, 2007), the following functional corresponding to (f) has been introduce

$$Q(x, \lambda, \xi) := \langle g(x), \xi \rangle - \lambda \langle b, \xi \rangle, \quad (x, \xi) \in Q \times \mathbb{R}^n.$$

This functional has been called there *extended functional* due to the fact that it is defined on the extended space $Q \times \mathbb{R}^n$. In more general cases, for instance if we allow for function

$\langle b, \xi \rangle$ to be equal zero, the zero set $Q(x, \lambda, \xi) = 0$ of this functional can be used for finding bifurcations. Consider the following quotient

$$\lambda(x, \xi) = \frac{\langle g(x), \xi \rangle}{\langle h(x), \xi \rangle}, \quad \langle h(x), \xi \rangle \neq 0, \ (x, \xi) \in Q \times \mathbb{R}^n, \tag{14}$$

which is obtained from $Q(x, \lambda, \xi) = 0$ by resolving with respect to λ.

It is natural to call this quotient as *extended quotient* or may be better to call as *extended Collatz-Wieland quotient*. Notice that the so-called Collatz-Wieland quotient in linear theory of positive matrix A is defined as follows

$$\lambda(x, i) = \frac{\langle Ax, e_i \rangle}{\langle x, e_i \rangle}, \quad x \in (\mathbb{R}^+)^n.$$

whereas with respect to our theory the corresponding extended Collatz-Wieland quotient is

$$\lambda(x, \xi) = \frac{\langle Ax, \xi \rangle}{\langle x, \xi \rangle}, \quad \langle h(x), \xi \rangle \neq 0, \ (x, \xi) \in (\mathbb{R}^+)^n \times \mathbb{R}^n,$$

which is defined on the extended space $(\mathbb{R}^+)^n \times \mathbb{R}^n$. The basic idea of the extended functional method (IL'YASOV, 2007) consists in finding a functional which stationary points correspond with the saddle-node bifurcations (bifurcations point for short) of solutions of the system. Following this idea we introduce the so-called *extended functional quotient*

$$\lambda(x, \xi) = \frac{\langle g(x), \xi \rangle}{\langle b, \xi \rangle}, \quad \langle b, \xi \rangle \neq 0, x \in Q, \ \xi \in \mathbb{R}^n \setminus 0. \tag{15}$$

A remarkable feature of this function is that the set of its stationary points corresponds to the set of bifurcation points of (f). Indeed, assume that $\bar{\lambda} = \lambda(\bar{x}, \bar{\xi})$ is a critical value of $\lambda(x, \xi)$ which corresponds to the stationary point $(\bar{x}, \bar{\xi}) \in Q \times (\mathbb{R}^n \setminus 0)$. Then calculating the derivatives yields

$$\nabla_\xi \lambda(\bar{x}, \bar{\xi}) = \frac{1}{\langle b, \bar{\xi} \rangle}(g(\bar{x}) - \bar{\lambda}b) = 0, \tag{16}$$

$$\nabla_x \lambda(\bar{x}, \bar{\xi}) = \frac{1}{\langle b, \bar{\xi} \rangle}(J_x g(\bar{x}))^T \bar{\xi} = 0, \tag{17}$$

Since $\frac{1}{\langle b, \bar{\xi} \rangle} \neq 0$, this implies:

$$(g(\bar{x}) - \bar{\lambda}b) = 0,$$
$$J_x g(\bar{x})^T \bar{\xi} = 0,$$

Taking into account that $(J_x g(\bar{x}))^T = (J_x f(\bar{x}, \bar{\lambda}))^T$ we obtain (18) which implies:

$$\begin{cases} f(\bar{x}, \bar{\lambda}) = 0, \\ (J_x f(\bar{x}, \bar{\lambda}))^T (\bar{\xi}) = 0, \end{cases} \tag{18}$$

with $\bar{\lambda} = \lambda(\bar{x}, \bar{\xi})$ and where

$$(J_x f(x, \lambda))^T = (\nabla_x f_i)_{1 \leq i \leq n}.$$

is the transpose of the Jacobian matrix $J_x f(x, \lambda)$ of $f(x, \lambda)$, i.e.,

$$J_x f(x, \lambda) = (\frac{\partial f}{\partial x_i})_{1 \leq i \leq n} = \begin{vmatrix} \frac{\partial f_1}{\partial x_1} & \cdots & \frac{\partial f_1}{\partial x_n} \\ \vdots & \ddots & \vdots \\ \frac{\partial f_n}{\partial x_1} & \cdots & \frac{\partial f_n}{\partial x_n} \end{vmatrix}$$

Evidently, if (18) is satisfied then there is $\bar{\zeta} \in \mathbb{R}^n \setminus 0$ such that $(\bar{x}, \bar{\zeta})$ satisfies to the branching system (see (ABBOTT et al., 1977; DOEDEL; KELLER; KERNEVEZ, 1991; KELLER, 1977; SEYDEL, 2009))

$$\begin{cases} f(\bar{x}, \bar{\lambda}) = 0, \\ (J_x f(\bar{\lambda}, \bar{x}))(\bar{\zeta}) = 0. \end{cases} \tag{19}$$

Since every saddle-node bifurcation point $(\bar{x}, \bar{\lambda})$ satisfies (19) with some bifurcation vector $\bar{\zeta} \in \mathbb{R}^n \setminus 0$, we conclude that any methods of finding bifurcations, including such as direct and continuation methods (AJJARAPU; CHRISTY, 1992; CHIANG et al., 1995; ALVARADO, 1989; AJJARAPU, 1991; CANIZARES; ALVARADO, 1993; DOBSON; LU, 1993) are inherently ones of the particular approaches of finding the stationary points of the extended quotient $\lambda(x, \xi)$. Hereafter, we call (18) the *conjugate branching system* while $\bar{\xi}$ we call a *conjugate bifurcation vector* corresponding to $\bar{x}$, and we call $(\bar{x}, \bar{\xi})$ the *simple stationary point* of $\lambda(x, \xi)$ if (18) holds true and $Ker(J_x f(\bar{x}, \bar{\lambda}))^T = \text{span } \{\bar{\xi}\}$.

It appears, that under general conditions, stationary points of $\lambda(x, \xi)$ corresponding to bifurcation points of (f), are defined by the saddle points of the function. However, saddle points are difficult for detecting using direct variational methods such as minimization or maximization of $\lambda(x, \xi)$.

Approaches based on Newton's method in some cases, can be better alternatives. In the theory of finding bifurcations, these type of methods are often called direct (see e.g., (SEYDEL, 2009)) . The extended functional approch allows introducing the direct method in a more unified form. Indeed, consider

$$F(y) = \begin{bmatrix} \nabla_\xi \lambda(x, \xi) \\ \nabla_x \lambda(x, \xi) \end{bmatrix} = 0, \quad \text{where} \quad y = \begin{bmatrix} x \\ \xi \end{bmatrix}, \tag{20}$$

and

$$\nabla_\xi \lambda(x, \xi) = \frac{1}{\langle b, \xi \rangle}(g(x) - \lambda(x, \xi)b),$$

$$\nabla_x \lambda(x, \xi) = \frac{1}{\langle b, \xi \rangle} \nabla_x g(x) \xi.$$

Thus, in the framework of the extended functional approach, bifurcation points of (f) can be calculated by applying the Newton method to $F(y) = 0$ similar to the direct

method (see e.g., (ALVARADO, 1989; AJJARAPU, 1991; CANIZARES; ALVARADO, 1993; DOBSON; LU, 1993; SEYDEL, 2009)). But now the situation is different that is we have only $2n$ variables and $2n$ equations and we would need only to guess a reasonable initial point (x_0, ξ_0) to start the iterative process to apply the direct method. Notice that the standard approach of the direct method deals with $2n + 1$ equations and in addition, one must guess the appropriate initial value λ_0.

3.1.1   Nonsmooth bifurcation functional

A bifurcation point (x^*, λ^*) is said to be maximal of (f) in Q if $\lambda' \leq \lambda^*$ for any other bifurcation (x', λ') of (f) in Q. It is important to point out, that throughout the thesis, the maximum bifurcation point of (f) corresponds to a constant parametric growth, as a simplifying basis to introduce the extended functional. It, therefore, understandably represents the maximum loading capacity of the power system for a constant direction of load growth.

From now on, we shall assume that $b_i > 0$, for all $i \in \{1, \ldots n\}$. Obviously, if $b_i \neq 0$, for all $i \in \{1, \ldots n\}$, one can always achieve this condition by multiplying on (-1) equations in (f).

Consider the following maximin problem

$$\lambda^* = \max_{x \in Q} \inf_{\xi \in (\mathbb{R}^+)^n} \lambda(x, \xi). \tag{21}$$

From (IL'YASOV; IVANOV, 2016) we have:

Lemma 1. *Assume that there exists a maximizer x^* of* (21). *Let ξ^* be the corresponding conjugate bifurcation vector. Suppose that (x^*, ξ^*) is a simple stationary point of $\lambda(x, \xi)$. Then (x^*, λ^*) is a maximal bifurcation point of (f) in Q.*

It turns out that problem (21) is equivalent to a non-smooth optimization problem. Indeed, let us define the so-called *bifurcation function*

$$\lambda(x) = \inf_{\xi \in (\mathbb{R}^+)^n} \lambda(x, \xi), \quad x \in Q.$$

Then by (IL'YASOV, 2007; IVANOV; IL'YASOV, 2013) the following identity is satisfied

$$\lambda(x) = \min_{i=1,\ldots,n} \frac{\langle g(x), e_i \rangle}{\langle b, e_i \rangle} = \min_{i=1,\ldots,n} r_i(x), \quad x \in Q, \tag{22}$$

where $r_i(x) = \langle g(x), e_i \rangle / \langle b, e_i \rangle \equiv g_i(x)/b_i$, $i = 1, 2, ..., n$.
Since $r_i \in C^1(Q)$, $i = 1, 2, ..., n$, this implies that $\lambda(x)$ *is a piecewise continuously differentiable function.* Thus, problem (21) is equivalent to the following nonsmooth optimization problem $\lambda^* = \max_{x \in Q} \lambda(x)$. Following (DEMYANOV et al., 2013), let us define

$$\partial \lambda(x) := conv\{\nabla r_i(x) : i \in N(x)\} \tag{23}$$

where "conv" denotes the convex hull of a set, $N(x) = \{i \in [1:n] : r_i(x) = \lambda(x)\}$, and $|N(x)|$ denotes the number of elements in $N(x)$. A point $\bar{x} \in Q$ is said to be *stationary point* of $\lambda(x)$ if $0 \in \partial\lambda(\bar{x})$ or the same if there holds

$$\sum_{i \in N(\bar{x})} \nabla r_i(\bar{x})\bar{\xi}_i = 0$$

with some $\bar{\xi} \in (\mathbb{R}^+)^{N(\bar{x})}\backslash 0$. Notice that in the case $|N(\bar{x})| = n$, this yields $(J_x f(\bar{x}, \bar{\lambda}))^T(\bar{\xi}) = 0$ and by (22) one has $f(\bar{x}, \bar{\lambda}) = 0$. Thus, any stationary point $\bar{x}$ of $\lambda(x)$ such that $|N(\bar{x})| = n$ satisfies to conjugate branching system (18). It can be make the conjecture that for the power balance system, any stationary point $\bar{x}$ satisfies $|N(\bar{x})| = n$. Then we have:

❏ *The maximum bifurcation point of the power balance system* (f) *and therefore the maximum loading capacity of the power system is located at the maximizing point of the nonsmooth function* $\lambda(x) = \min_i r_i(x)$.

Nonsmooth optimization deals with optimization problems where objective functions have discontinuous gradients and it has been intensively developing over the past few decades. There is a large amount of literature on nonsmooth optimization algorithms, and there are various numerical methods for such problems: subgradient, cutting plane, bundle, gradient sampling methods, etc. (see e.g., (BAGIROV; KARMITSA; MÄKELÄ, 2014; DEM'YANOV; MALOZEMOV, ; KIWIEL, 2006)). All these methods have their supporters and advantages, which may depend on the type of problems under consideration.

Given the power balance system (f) has not yet been investigated under the framework of the theory of nonsmooth optimization, it makes sense to test the known methods of this theory to determine the optimal one.

In the present work, we test the subgradient method for (f). In this regard, it makes sense to emphasize that the continuation approach of finding the bifurcation, as it has been shown in (IL'YASOV; IVANOV, 2016) (see also below Remark 1), is a special case of the subgradient method.

3.2 Algorithm

To find the maximizing point of $\lambda(x)$, we apply the subgradient method using an approach introduced in (IL'YASOV; IVANOV, 2016; IVANOV; IL'YASOV, 2013). By (DEM'YANOV; MALOZEMOV, ; ROCKAFELLAR, 1984), $\lambda(x)$ is a directionally differentiable function in Q with respect to any vector $d \in \mathbb{R}^n$ and the directional derivative is defined by

$$\lambda'(x; d) = \min_i\{\langle \nabla r_i(x), d \rangle : i \in N(x)\}. \tag{24}$$

Following (DEM'YANOV; MALOZEMOV, ; ROCKAFELLAR, 1984) we call a maximizer $\hat{d}(u) \in \mathbb{R}^n$ of

$$\hat{\sigma}(x) = \lambda'(x; \hat{d}(x)) = \max\{\lambda'(x; d) : ||d|| = 1\} \tag{25}$$

(if $\hat{\sigma}(x) > 0$) a *direction of steepest ascent* of $\lambda(x)$ at $x \in Q$. In this case, we define a gradient of $\lambda(x)$ as follows

$$\nabla\lambda(x) := \lambda'(x; \hat{d}(x)) \cdot \hat{d}(x) \equiv \hat{\sigma}(x) \cdot \hat{d}(x).$$

Observe that by Demyanov-Malozemov's Theorem (DEM'YANOV; MALOZEMOV,), $\nabla\lambda(x)$ is a nearest point from the origin 0_n to the convex set $\partial\lambda(x)$. Introduce matrices

$$A_{N(x)} = \left(\nabla r_{i_k}(x)\right)^T_{1 \leq k \leq |N(x)|}, \ \Gamma_{N(x)} = A^T_{N(x)} A_{N(x)},$$

where $i_1, ..., i_N \in N(x)$ is an arrangement of the set $N(x)$ such that $i_1 < i_2 < \ldots < i_N$. From (IL'YASOV; IVANOV, 2016; IVANOV; IL'YASOV, 2013) it follows that the maximization problem (25) is equivalent to the following quadratic programming problem

$$\hat{\sigma}^2(x) = \min_\alpha\{\alpha^T \Gamma_{N(x)} \alpha : \ \alpha \in \mathbb{R}^{N(x)}, \tag{26}$$

$$\sum_{i=1}^{N(x)} \alpha_i = 1, \ \ \alpha_i \geq 0, \ i = 1, ..., N(x)\},$$

so that if $\hat{\alpha}(x)$ is a minimizer of (26), then

$$\nabla\lambda(x) = \sum_{k=1}^{N} \hat{\alpha}_k \nabla f_{i_k}(x) \equiv A_{N(x)} \hat{\alpha}(x), \tag{27}$$

and

$$\hat{d}(x) = \nabla\lambda(x)/\hat{\sigma}(x) \equiv \frac{A_{N(x)} \hat{\alpha}(x)}{||A_{N(x)} \hat{\alpha}(x)||} \tag{28}$$

is a maximizer of (25) (IVANOV; IL'YASOV, 2013).

An important property of $\hat{\sigma}(x)$ (see (DEM'YANOV; MALOZEMOV, ; DEMYANOV et al., 2013)) is that if $\hat{\sigma}(x) > 0$, then there exist $\tau_0 > 0$ such that

$$\lambda(x + \tau\hat{d}(x)) > \lambda(x)$$

for any $\tau \in (0, \tau_0)$. Furthermore (see (IL'YASOV; IVANOV, 2016)) if $x^* \in Q$ is a maximizer of $\lambda(x)$, then the necessary conditions of optimality $\hat{\sigma}(x^*) = 0$ is satisfied and there exists $\xi^* \in (\overline{\mathbb{R}^+})^n \setminus 0$ such that $\xi^* \in Ker(J_x f^T(x^*, \lambda^*)^T)$.

Accordingly, one can introduce the iteration formula for steepest ascent direction method (see e.g., (IVANOV; IL'YASOV, 2013))

$$x_{k+1} = x_k + t_k \frac{\hat{d}(x_k)}{\|\hat{d}(x_k)\|}.$$

Here $t_k > 0$ is a predetermined step size. However, this approach has a certain deficiency, namely the finding of the steepest ascent direction by (26) is time-consuming.
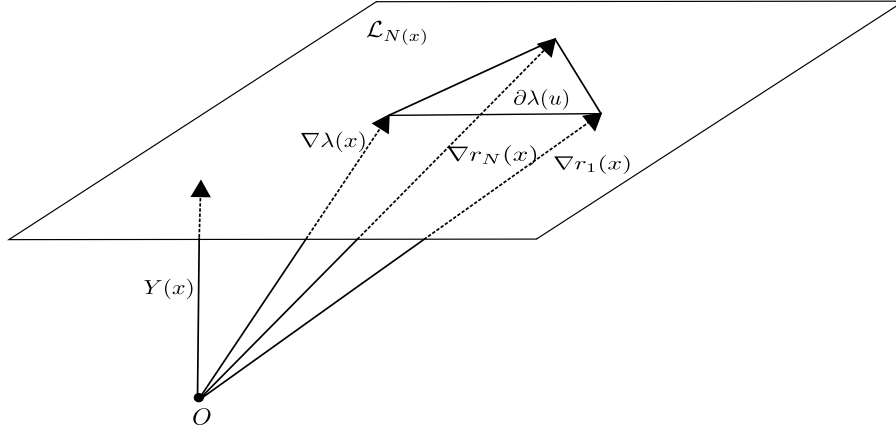
Figure 6 – Quasi-direction of steepest ascent $Y(x)$ and direction of steepest ascent $\nabla\lambda(x)$

To avoid this, the authors in (IL'YASOV; IVANOV, 2016), proposed the so-called method of quasi-direction of steepest ascent. In this way, the quasi-direction of steepest ascent $Y(x)$ is determined by solving a system of linear equations which is less time-consuming than solving (26).

Let us shortly describe the ideas of this method. For $\delta \in \mathbb{R}$, consider the following system of equations

$$
\begin{cases}
\Gamma_{N(x)}\alpha = \delta \cdot 1_{|N(x)|}, \\
\sum\limits_{i=1}^{|N(x)|} \alpha_i = 1,
\end{cases}
\tag{29}
$$

where $\alpha = (\alpha_1, ..., \alpha_{|N(x)|})^T$.

Assume that $|N(x)| > 1$. Consider the affine space

$$
L_{N(x)} = \{v = \sum_{i \in N(x)} \beta_i \nabla r_i(x) : \sum_{i \in N(x)} \beta_i = 1\}.
$$

Introduce $Y(x) = A_{N(x)}^T \alpha(x)$, where $\alpha(x)$ satisfies (29). Observe, if $\delta > 0$, then (29) implies

$$
\langle Y(x), \nabla r_i(x) \rangle = \langle A_{N(x)}\alpha, \nabla r_i(x) \rangle = \langle \Gamma_{N(x)}\alpha, e_i \rangle
\tag{30}
$$

$\forall i \in N(x)$. From this it follows that $Y(x)$ is an orthogonal vector to $L_{N(x)}$ (see (IL'YASOV; IVANOV, 2016)) and thus $Y(x)$ is the nearest point from the origin $0_n \in \mathbb{R}^n$ to the affine space $L_{N(x)}$. Recall that $\nabla\lambda(x)$ is a nearest point from the origin 0_n to the convex set $\partial\lambda(x)$. Hence and since $\partial\lambda(x)$ lies on $L_{N(x)}$, it follows that the necessary conditions of optimality $\hat{\sigma}(x^*) = 0$, i.e., $0 \in \partial\lambda(x)$, entails $Y(x^*) = 0$. See Figure 6.

Furthermore, the following main lemma holds (see (IL'YASOV; IVANOV, 2016))

Lemma 2. *Let $x \in Q$ and assume that (α, δ) is a solution of (29). Then*

a) *If $\delta = 0$, then $|N(x)| = n$ and $\alpha_k \neq 0$, $\forall k = 1, ..., n$.*

b) *If $\delta = 0$ and $\alpha_k > 0$, $\forall k = 1, ..., n$, then $\hat{\sigma}(x) = 0$, and there exists $\xi \in (\overline{\mathbb{R}^+})^n \setminus 0$ such that $\xi \in Ker(J_x f(x, \lambda))^T$ with $\lambda = \lambda(x, \xi)$.*

c) *If $\delta = 0$ and there exist subsets $N_1(x), N_2(x)$ such that $N_1(x) \cup N_2(x) = N(x)$ and*
$\alpha_k > 0, \forall k \in N_1(x)$, whereas $\alpha_k \leq 0, \forall k \in N_2(x)$, then $\nabla \lambda(x)$ lies on the boundary
$\partial_{N_1(x)} \lambda(x)$ of $\partial \lambda(x)$.

The following convergence iteration by quasi-direction of steepest ascent method can be introduced:

$$x_{k+1} = x_k + \tau_k \frac{Y(x_k)}{\|Y(x_k)\|}$$

where $\tau_k > 0$ is a predetermined step size (IL'YASOV; IVANOV, 2016). Below, the finding of the maximal SNB point of (f) will be carried out with a given accuracy. Let us give the corresponding definitions. Following (IL'YASOV; IVANOV, 2016), we say that x is a solution of (f) with accuracy $\varepsilon > 0$, if

$$|r_i(x) - \lambda(x)| < \varepsilon \quad \text{for all} \quad i = 1, 2, ..., n. \tag{31}$$

Denote $N_\varepsilon(x) = \{i \in [1 : n] : |r_i(x) - \lambda(x)| < \varepsilon\}$. Then x is a solution of (f) with accuracy $\varepsilon > 0$ if and only if $|N_\varepsilon(u)| = n$.

Let $\varepsilon_0 > 0, \delta_0 > 0$. We call $x^*_{(\varepsilon_0, \delta_0)}$ the δ_0- SNB point of (f) with accuracy ε_0 if

(i) $|N_{\varepsilon_0}(x^*_{(\varepsilon_0, \delta_0)})| = n$,

(ii) $\Gamma_{N_{\varepsilon_0}(x^*_{(\varepsilon_0, \delta_0)})} \alpha = \delta \cdot 1_{|N_{\varepsilon_0}(x^*_{(\varepsilon_0, \delta_0)})|}$,
for $\delta \in (0, \delta_0)$ and $\alpha \in \mathbb{R}_+^{|N_{\varepsilon_0}(x^*_{(\varepsilon_0, \delta_0)})|}$ such that $\sum_{1 \leq i \leq |N_{\varepsilon_0}(x^*_{(\varepsilon_0, \delta_0)})|} \alpha_i = 1$.

The corresponding pseudo-code of the quasi-direction of the steepest ascent (QDSA) algorithm for finding the δ_0- SNB point with a given accuracy ϵ_0 is presented in the next section. The algorithm enables the finite cyclic reduction of ϵ and δ. The convergence of this algorithm is discussed in (IL'YASOV; IVANOV, 2016).

Remark 1. *Assume $N(x) = n$, then*

$$\lambda(x) = \frac{g_i(x)}{b_i}, \quad \forall i = 1, \dots, n,$$

which means that x satisfies (f) with $\lambda = \lambda(x)$ and thus, the point x lies on the branch of the solutions of (f). On the other hand, if $N(x) = n$ and (α, δ) solves (29), then:

$$A(x) A^T(x) \alpha = \delta 1_n$$

Now denoting $\dot{x} = \frac{A^T(x)\alpha}{\delta}$, we obtain (see (IVANOV; IL'YASOV, 2013)) the Davidenko-Abbott system

$$J_x f(x, \lambda)) \dot{x} = -f_\lambda(x, \lambda), \tag{32}$$

which lies at the core of the continuation methods (see e.g. (KELLER, 1977; SEYDEL, 2009)). Notice that equality $Y(x) = \dot{x} \delta$ implies that the quasi-direction of steepest ascent $Y(x)$ is collinear with the tangent vector $\dot{x}$ to the curve of the branch of the solutions of (f). Thus, the predictor step by the tangent vector in the continuation approach is, in fact, a particular case of the quasi-direction of the steepest ascent method when $|N(x)| = n$.

3.2.1 Pseudo-Code for the Quasi-Direction of Steepest Ascent Algorithm (QDSA)

Algorithm 1 The QDSA Pseudo-Code

1: Set an initial point x^0 and accuracies $\epsilon_0 > 0$ and $\delta_0 > 0$

For $k = 0, 1, 2....$ until the saddle-node bifurcation point (x^*, λ^*) is found.

2: Compute

$$\lambda(x^k) = \min_i r_i(x^k)$$

$$\mu(x^k) = \max_i r_i(x^k)$$

Compute

$$\epsilon = (\mu(x^k) - \lambda(x^k))/2$$

3: Input the set of indexes

$$N_\epsilon(x^k) = \{i \in \{1 : n\} : |r_i(x^k) - \lambda(x^k)| < \epsilon\},$$

$$N = |N_\epsilon(x^k)|$$

4: Find δ^k and α^k by solving

$$\mathcal{M}_{N_\epsilon(x^k)} t^k = q_N,$$

where

$$\mathcal{M}_{N_\epsilon(x^k)} = \begin{pmatrix} \Gamma_{N_\epsilon(x^k)} & -1_{N_\epsilon(x^k)} \\ 1^T_{N_\epsilon(x^k)} & 0 \end{pmatrix}.$$

$$\Gamma_{N_\epsilon(x^k)} = A^T_{N_\epsilon(x^k)} A_{N_\epsilon(x^k)}, \ t^k = \begin{pmatrix} \alpha^k \\ \delta^k \end{pmatrix}, \ q_N = \begin{pmatrix} 0 \\ 1 \end{pmatrix}$$

5: If $\delta^k < \delta_0$, then go to Step 6, otherwise

a) Compute the quasi-direction of steepest ascent

$$y^k = \frac{Y^k}{\|Y^k\|}, \ Y^k = A^T_{N_\epsilon(x^k)} \alpha^k$$

b) Find the step length τ^k by the *golden search rule* applied to

$$\tau^k = arg \max\{\min_i r_i(x^k + \tau y^k)\}, \ \ \tau > 0$$

c) Compute $x^{k+1} = x^k + \tau^k y^k$ and return to Step 2

6: If $\epsilon < \epsilon_0$, then go to step 7, otherwise $\epsilon = \epsilon/2$ and return to step 3

7: If $N = n$, Output the bifurcation point $x^*_{(\epsilon,\delta)}$ and $\lambda^*_{(\epsilon,\delta)}$, otherwise $\delta_0 = \delta_0/2$ and return to step 6

3.3   Study Cases

In this section, we present the performance of the EFM applied on various tasks and the comparison with CPF and PoC method. The IEEE 14, 30, 57 and 118 test systems are used for simulations ignoring reactive power limits of generators. The study cases are divided into five sections:

❑ Testing various initial points x^0.

❑ Testing large λ cases.

❑ Tracking performance of the proposed method.

❑ Infeasible Power Flow $(0 < \lambda < 1)$.

❑ The EFM providing x^0 for PoC.

3.3.1   Testing various initial points x^0

The state vector x is composed of n unknown variables $(n_{bus} + n_{pq} - 1 = n)$, where n_{bus} is the number of buses and n_{pq} is the number of PQ type buses . The first n_{pq} elements of the vector x represent voltage modules $\bar{V} := [v_1, \ldots, v_{n_{pq}}]$, followed by voltage angles $\bar{\theta} := [\theta_1, \ldots, \theta_{n_{bus}-1}]$, so that $x = [\bar{V}, \bar{\theta}]^T$.

Four initial guess points x^0 are used to start the algorithm:

❑ $x^0 = [\bar{1}, \bar{0}]^T$ (Flat start)

❑ $\lambda(x^0) = 1$ (Equilibrium base case point)

❑ $x^0 = [\bar{0.5}, \frac{\bar{-\pi}}{10}]^T$

❑ $x^0 = [\bar{0.5}, \frac{\bar{-\pi}}{6}]^T$

In all scenarios, the performance is compared with the Continuation Power Flow and PoC Methods, using the open-access Matlab software PSAT (MILANO, 2005).

The EFM was implemented in MatLab R2015. For the Continuation Power Flow simulations on PSAT, the following settings were applied:

❑ Stop criterion: At Bifurcation point.

❑ Correction method: Perpendicular intersection.

❑ Adaptive Step Size with different initial values in order to not exceed 50 iterations (default).

Table 1 – Comparison between methods; IEEE 14-bus system

	EFM		CPF-PSAT			PoC-PSAT	
Case	λ	Time [s]	λ	Time [s]	Step Size	λ	Time [s]
$x^0 = [\bar{1}, \bar{0}]^T$	3.87	0.61	3.87	0.41	0.5	3.87	0.14
$\lambda(x^0) = 1$	3.87	0.84	3.87	0.31	0.5	3.87	0.14
$x^0 = [\bar{0.5}, \frac{\bar{-\pi}}{10}]^T$	3.87	0.73	NC[a]		0.5	NC[a]	
$x^0 = [\bar{0.5}, \frac{\bar{-\pi}}{6}]^T$	3.87	0.73	NC[a]		0.5	NC[a]	

[a] Not Converged;

Table 2 – Comparison between methods; IEEE 30-bus system

	EFM		CPF-PSAT			PoC-PSAT	
Case	λ	Time [s]	λ	Time [s]	Step Size	λ	Time [s]
$x^0 = [\bar{1}, \bar{0}]^T$	2.52	1.7	2.52	1.52	0.5	2.52	0.29
$\lambda(x^0) = 1$	2.52	4.9	2.52	1.42	0.5	2.52	0.29
$x^0 = [\bar{0.5}, \frac{\bar{-\pi}}{10}]^T$	2.52	2.7	NC[a]		0.5	NC[a]	
$x^0 = [\bar{0.5}, \frac{\bar{-\pi}}{6}]^T$	2.52	4.5	NC[a]		0.5	NC[a]	

[a] Not Converged;

Table 3 – Comparison between methods; IEEE 57-bus system

	EFM		CPF-PSAT			PoC-PSAT	
Case	λ	Time [s]	λ	Time [s]	Step Size	λ	Time [s]
$x^0 = [\bar{1}, \bar{0}]^T$	1.55	9.1	1.55	0.937	0.1	1.55	0.15
$\lambda(x^0) = 1$	1.56	11.1	1.55	0.837	0.1	1.55	0.15
$x^0 = [\bar{0.5}, \frac{\bar{-\pi}}{10}]^T$	1.55	112.8	NC[a]		0.5	NC[a]	
$x^0 = [\bar{0.5}, \frac{\bar{-\pi}}{6}]^T$	1.55	115.6	NC[a]		0.5	NC[a]	

[a] Not Converged;

For the PoC on PSAT, all simulations begin running CPF to get a close initial start point since otherwise, none of the cases converge. Simulations were run on an Intel i7 of 3.2 GHz CPU and 16 GB of RAM.

As shown in Tables 1,2,3, and 4, the EFM was the only one that converged successfully and found the solutions using initial guess points $x^0 = [\bar{0.5}, \frac{\bar{-\pi}}{10}]^T$ and $x^0 = [\bar{0.5}, \frac{\bar{-\pi}}{6}]^T$. No case converged with the PoC method using a flat start, and the converged cases used a suitable initial point provided by the CPF method.

Fig. 7 shows the schematic representation of the iterative procedure of the EFM to find the SNB using a flat start as the initial guess point.

3.3.2 Testing large λ cases

Six random load level scenarios of the IEEE 30-bus system were simulated, decreasing the system's total load in the subsequent scenario to increase the voltage Stability Margin (VSM) and to stress the methods. Table 5 shows that the PoC is the fastest method among

Table 4 – Comparison between methods; IEEE 118-bus system

Case	EFM		CPF-PSAT			PoC-PSAT	
	λ	Time [s]	λ	Time [s]	Step Size	λ	Time [s]
$x^0 = [\bar{1}, \bar{0}]^T$	2.05	74.5	2.05	1.12	0.5	2.05	0.2
$\lambda(x^0) = 1$	2.05	76.8	2.05	1.02	0.5	2.05	0.2
$x^0 = [\bar{0.5}, \frac{-\pi}{10}]^T$	2.05	235.7	NC[a]		0.5	NC[a]	
$x^0 = [\bar{0.5}, \frac{-\pi}{6}]^T$	2.05	256.8	NC[a]		0.5	NC[a]	

[a] Not Converged;
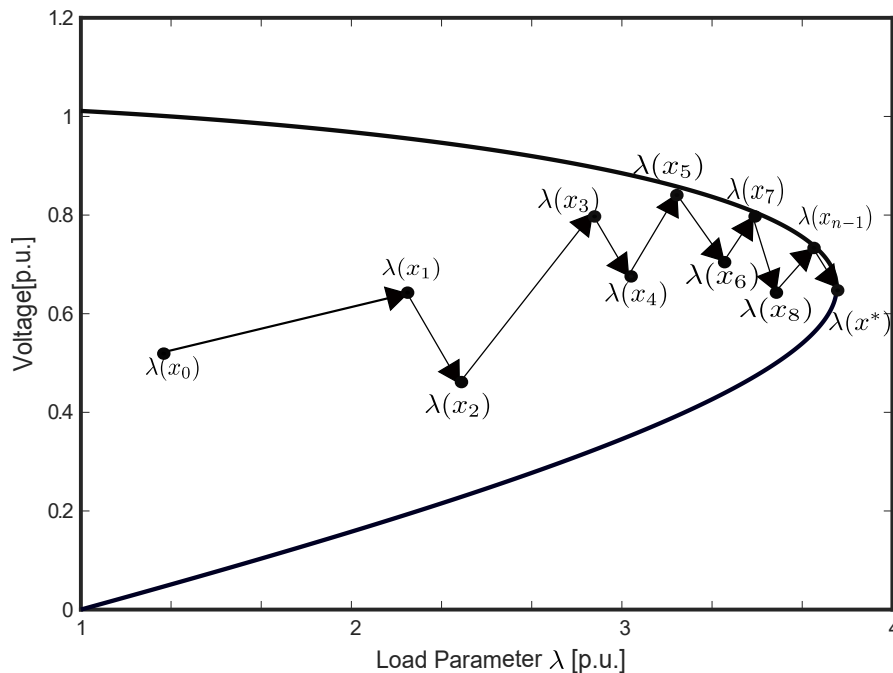
Figure 7 – Representation of the iterative procedure to find the SNB by the EFM.

all (with initial guess provided by the CPF method). On the other hand, EFM has shown better performance than CPF for large λ.

The CPF is time-consuming for cases with large λ (Base Case far from SNB), while the EFM seems to have a constant-time performance independent of λ size.

Even with the initial guess provided by CPF, two cases did not converge using the PoC method, and one converged case yielded a wrong answer.

3.3.3   Tracking Performance of the Extended Functional Method

We compared the EFM and the PoC method tracking an SNB point shifted by a network contingency using the SNB point before perturbation as the initial guess for finding the new SNB. The CPF method does not work in this case because it is dependent on the base case convergence. For testing tracking performance, two perturbations were introduced in Case 1 of the IEEE 30-bus system. The first one causes the SNB point displacement due to the outage of two capacitors (buses 10 and 14). This contingency

Table 5 – Testing large λ cases; $x^0 = [\bar{1}, \bar{0}]^T$ (IEEE 30-bus system)

| | EFM | | CPF-PSAT | | | PoC-PSAT | |
Case	λ	Time [s]	λ	Time [s]	Step Size	λ	Time [s]
1	2.52	1.7	2.52	1.52	0.5	2.52	0.29
2	4.85	1.9	4.85	1.08	0.5	4.85	0.2386
3	6.00	2.1	6.00	0.68	0.5	6.00	0.2758
4	7.14	1.4	7.14	2.73	0.5	7.15	0.2385
5	9.67	1.3	9.68	1.73	2	NC[a]	NC[a]
6	13.87	1.7	13.87	2.6	2	WA[b]	WA[b]

[a] Not Converged;
[b] Wrong Answer

is considered a small perturbation since λ decreases less than 2% (from 2.52 to 2.48). The outage of line 2-5 causes the second displacement of the SNB. This contingency is considered a significant perturbation since λ decreases considerably (from 2.48 to 2.02). Table 6 shows that both the EFM and PoC method tracks the first SNB displacement successfully, being PoC faster than EFM. The second displacement is tracked successfully only by the EFM. Fig. 8 shows the schematic representation of the tracking procedure.

Table 6 – Tracking Performance of the EF Method - IEEE 30-bus system

| | | EFM | | PoC-PSAT | |
Case	x^0	λ	Time [s]	λ	Time [s]
Cont. 1	Base Case SNB	2.48	1.1	2.48	0.268
Cont. 2	Cont.1 SNB	2.02	1.4	NC[a]	NC[a]

[a] Not Converged;

3.3.4 Infeasible Power Flow ($0 < \lambda < 1$)

We tested an infeasible power flow in which the given load level is beyond the SNB point, and a physical solution does not exist. In this case, SNB point exists with a load level smaller than the given load level, so that the SNB point exists in the range $0 < \lambda < 1$. For testing an infeasible power flow, a severe contingency to case 1 of the IEEE 30-bus-system was applied. Generators 2, 3, 5, and 13 were set as PQ buses, generators 8 and 11 were set with 1 [p.u.] of voltage output, capacitors 10 and 24, lines 2-5, 6-8, and 14-15 were set out of service. This simulation converged successfully with the EFM yielding $\lambda = 0.84$. PoC method did not converge. Fig. 9 shows how the PV curve decreases to the infeasible region ($0 < \lambda < 1$) due to the severe contingency.
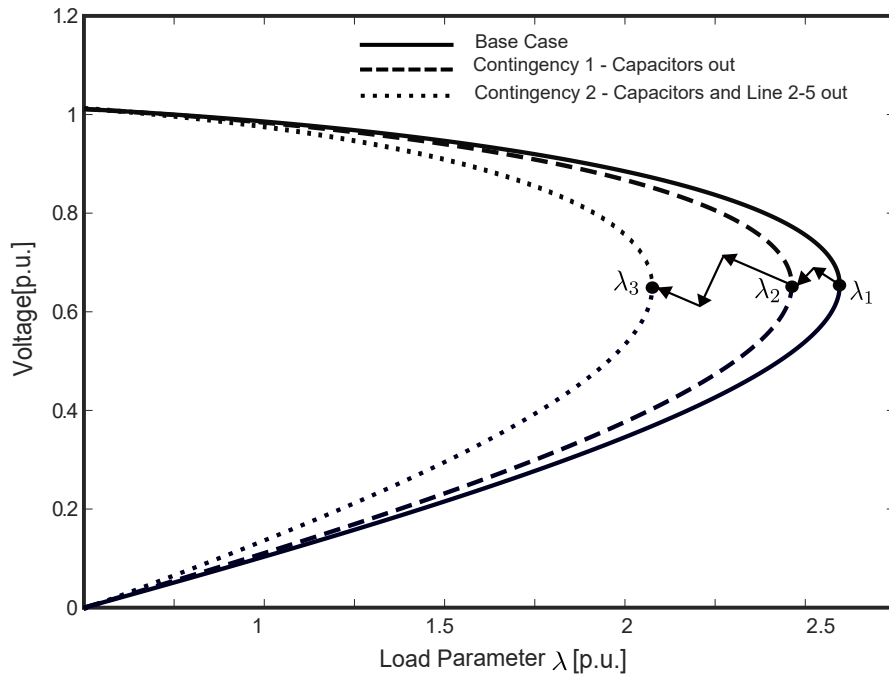
Figure 8 – Tracking SNB Point Scheme
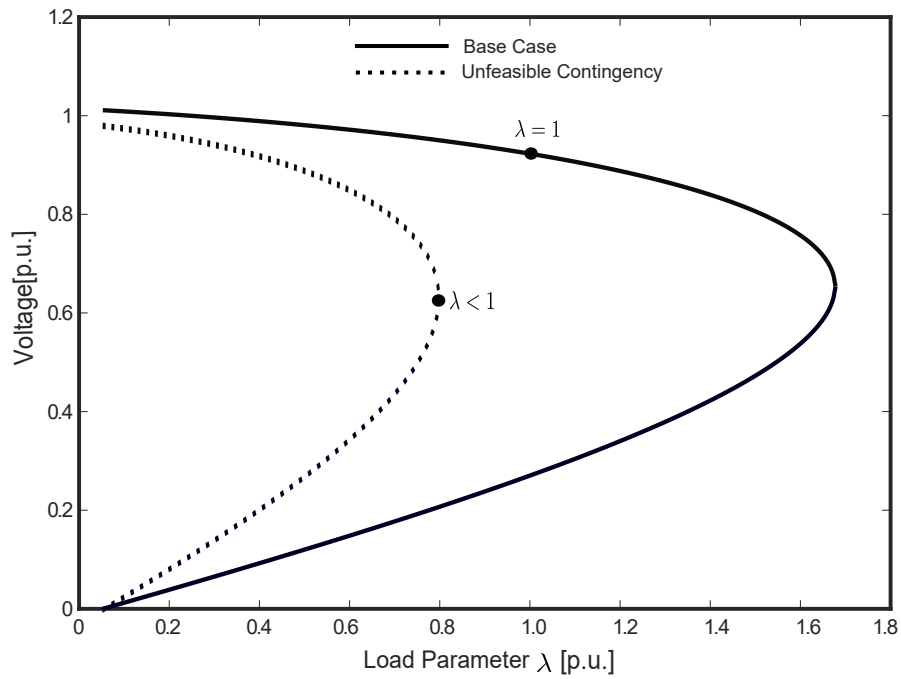
Figure 9 – Infeasible Contingency Case

3.3.5 EFM providing x^0 for PoC method

Finally, we tested the EFM, providing suitable x^0 for the PoC method. We tested Cases 5 and 6 of the IEEE 30-bus system, in which the PoC method did not converge with the initial guess point provided by the CPF method. The stop criterion for the EFM to provide suitable initial guess point are $|N(x^k)| = n$ and $\mu(x^k) - \lambda(x^k) < 5$. It is worth noting that the initial right eigenvector and λ for the PoC method can be provided by the EFM as well. Using the mentioned stop criterion, the EFM provided a suitable initial guess point for PoC convergence. Table 7 shows the total time of the two cases using both the EFM and PoC method.

Table 7 – EFM Providing x^0 for PoC method - IEEE 30-bus system

| | | EFM | PoC-PSAT | |
Case	λ	Time [s]	Time [s]	Total Time [s]
5	9.68	0.5	0.3	0.8
6	13.87	0.9	0.25	1.15

3.3.6 Discussion on the performance of the extended functional method

A new concept for finding saddle-node bifurcation points has been presented. The stationary points of the nonsmooth functional $\lambda(x)$ correspond to the saddle-node bifurcation point. A full range of nonsmooth optimization methods can be applied to find bifurcation points. Among these methods, the subgradient method for nonsmooth functions (QDSA algorithm) has been applied to find the maximal bifurcation point of power systems. As a result, the following achievements can be highlighted:

❏ It is the first time using the extended functional and introducing a variational function $\lambda(x)$ in a precise form in which stationary points correspond to the maximum loading capacity of the power system.

❏ We show that $\lambda(x)$ is nonsmooth, and thus any method of calculation of the maximum loading capacity of the power system deals with nonsmooth optimization. Notice that nonsmooth optimization is among the most challenging tasks in optimization.

Also, various features can be highlighted:

❏ Only a portion of the jacobian matrix of the system is used in each iteration because trajectory equilibrium points are not of interest. This feature decreases the computational cost of solving the linear system when finding the functional ξ.

❏ The iterations and time consumption are not proportional to the distance between the base to the SNB. In this way, the initial guess does not affect convergence even when the base case is far away from the SNB.

❏ Since the method only looks for the SNB, it can be considered a direct method but without the need for a close initial start point for λ and the left/right eigenvector.

❏ Unlike the CPF method, the computing time is not proportional to λ size.

❏ The EFM can also be used to find a suitable close initial start point to accelerate the PoC method.

❏ Unlike the PoC method, the EFM does not need an initial guess point close to the solution to ensure convergence. Instead, the EFM converges using an initial guess point away from the solution.

Voltage Control and Short-Term Stability

4.1 Introduction

Enforcing grid codes has become increasingly challenged by the growing penetration of renewable sources to achieve a net-zero carbon emission goal. In North America, grid codes require wind farms (WFs) with an aggregated nameplate capacity above 20MVA to provide ride-through capabilities, i.e., staying online during abnormal frequency/voltage disturbances (ELLIS et al., 2012). The low voltage ride-through (LVRT) capability aims to guarantee continuous injection while the system is under low voltage during a disturbance and a fast voltage recovery during the post-fault transient (YARAMASU et al., 2015; MULLANE; LIGHTBODY; YACAMINI, 2005). One can apply several techniques to achieve LVRT requirements, e.g., the double-fed induction generator (DFIG) can perform a continuous operation under low voltage for a short period. In this technique, the crowbar resistor and the DC-link chopper, protects the power converter, which has a restricted over-current limit (VIDAL et al., 2013; PANNELL; ATKINSON; ZAHAWI, 2010). After clearing a disturbance, the DFIG returns to normal operation, and the voltage should recover to its nominal value as fast as possible. Voltage stability is a critical issue during the entire process. If there is insufficient reactive power, a voltage collapse will cause the outage of the WF. To help with the reactive power (VAR) support during this critical transient, VAR compensators are being used, such as the Static Synchronous Compensator (STATCOM), Static Var Compensator (SVC), Static Var Generators (SVG) and Convertible Static Compensators (CSC) (HINGORANI; GYUGYI; EL-HAWARY, 2000; SALLES; FREITAS; MORELATO, 2004). In that regard, a dynamic reactive power reserve (DRPR) from VAR compensators criterion has been proposed during normal operation to ensure fast VAR availability for a successful ride through.

The strategies mentioned above are well established and have reached maturity. However, it is important to highlight at this point other aspects besides DRPR criterion that

plays an essential role in the continuous improvement of the LVRT. One of these aspects is the OC's role before the disturbance on a successful ride-through. This paper will demonstrate that the VAR reserves should be available not only at the medium voltage bus (from VAR compensators) but at every WF node. In other words, maximizing VAR reserves in the WF is necessary for a normal OC. In (ZHAO et al., 2016; ZHAO et al., 2017; GUO et al., 2015), a preventive control based on the SVC/CVG DRPR is presented. However, as stated before, DRPR from the VAR compensator might not be enough to improve LVRT capability. In (ZHAO et al., 2016; ZHAO et al., 2017), a Model predictive control-based voltage control (MPC) is proposed for a normal operation condition. However, a widely recognized shortcoming of MPC is that it is designed for applications with slow dynamics, while its performance in fast dynamics like those of inverter-based sources is not ideal due to communication latency.

Another important aspect is the behavior of the local controls after the disturbance to restore the voltage . After clearing the fault, the local set-point remains at pre-fault constant values, which are not adequate for post-fault conditions and will not restore the voltage properly as required by grid codes. Classical local controls such as PID controllers rely on local measurements without taking into account the capacity and the OC of the system, depriving an optimal and coordinated response of all the WF resources (LIN; LIU; ZHU, 2021). In (QIAO; HARLEY; VENAYAGAMOORTHY, 2009), dynamic programming and a radial basis neural network is proposed to restore the voltage of a DFIG-based WF after a disturbance. However, the WF is reduced to an equivalent DFIG machine, which can cause miscalculations because each DFIG has its own VAR limit. To improve LVRT capability, reinforcement learning is applied to control a VAR compensator like CSC and STATCOM (ZHOU; SWAIN; UKIL, 2019). Nonetheless, the limit of VAR of each individual wind generator is not taken into account. During the transient restoration period, ideally, all available reactive resources should coordinately inject VAR to restore the voltage as fast as possible. As a result, the set-points ideally should change during the short transient period accordingly to the OC and the availability of resources of each wind generator.

The ideal centralized response is physically limited due to communication delays between the local and centralized controllers, and the time needed to solve the optimization problem to obtain the set-points during the transient period (GUO et al., 2017). To tackle the limitations of local controllers and centralized communications, we propose a risk-aware learning framework that allows us to systematically reduce the worst-case prediction guaranteeing a safe voltage control. Using only local and other reachable measurements of interest, the data-driven local voltage control is able to quickly calculate the set-points during the post-fault transient. The non-linearities due to the combination of local Proportional Integral (PI) control over the VAR first-order dynamics, in addition to the effects on the system power flow, make a neural network (NN) a suitable tool for the

learning process. To train the NN, a data-set is obtained offline by performing an ideal (without computation and communication limitations) centralized model predictive control (MPC) that is an efficient multi-input-multi-output (MIMO) control strategy when system dynamics are taken into account.

Notation: Upper (lower) boldface symbols stand for matrices (vectors); $(\cdot)^{\top}$ stands for matrix transposition; $\| \cdot \|_2$ denotes the L_2-norm; Upper $(\bar{\cdot})$ and lower bars $(\underline{\cdot})$ stand for maximum and minimum limits respectively, and hat $(\hat{\cdot})$ stands for setpoint.

4.2   System Modeling
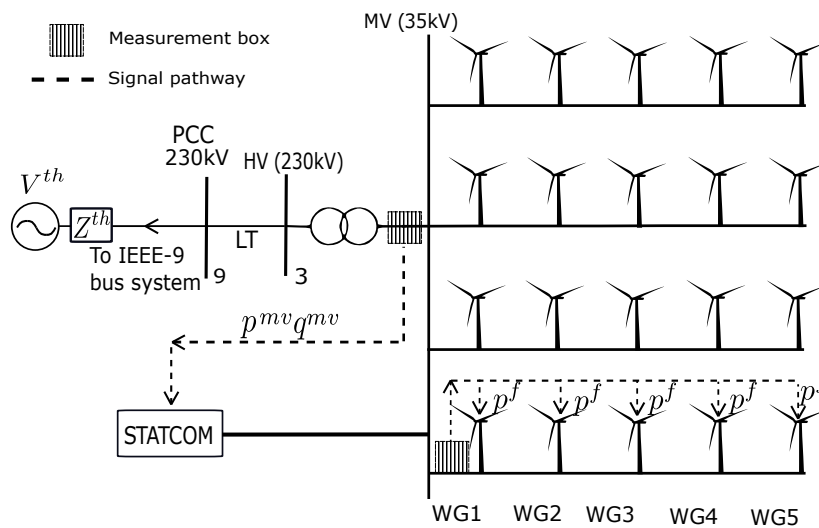
Figure 10 – Wind farm architecture. The pathway for measurement signals to be used for corrective control can be observed. The STATCOM uses total active power (p^{mv}) and VARs (q^{mv}) from the MV bus. Every WG uses the total active power (p^f) from the feeder it belongs.

Consider a WF consisting of a point of common coupling (PCC), a High Voltage (HV) bus, a Medium Voltage (MV) bus, and N wind generators (WGs). A STATCOM is connected to the MV bus for VAR support. The goal is to control the PCC voltage by coordinating the outputs from WGs and the STATCOM. Using the Thevenin equivalent of the external system model, one can use the Thevenin voltage v^{th} as the slack bus, as shown in Figure 10.

Thereby, the vector of WF nodal voltages $\boldsymbol{v}$ can be modeled as:

$$\boldsymbol{v} \approx \boldsymbol{R}\boldsymbol{p} + \boldsymbol{X}\boldsymbol{q} + v^{th}\mathbf{1}_N \tag{33}$$

with $\boldsymbol{v} = [v^{pcc}, v^{hv}, v^s, v_1^w, ..., v_N^w]^{\top}$, $\boldsymbol{p}$ and $\boldsymbol{q}$ as the vectors of active power and VAR injections, respectively. In addition, $\boldsymbol{R}$ and $\boldsymbol{X}$ represent the corresponding sensitivity matrices. For example, using the linearized DistFlow approximation (BARAN; WU, 1989), they can be respectively formed using the node-to-edge graph incidence matrix $\boldsymbol{M}$

(ZHU; LIU, 2015), as given by:

$$\boldsymbol{R} = 2(\boldsymbol{M}^{-1})^{\top}\mathrm{diag}(\boldsymbol{r})(\boldsymbol{M}^{-1}) \tag{34}$$

$$\boldsymbol{X} = 2(\boldsymbol{M}^{-1})^{\top}\mathrm{diag}(\boldsymbol{x})(\boldsymbol{M}^{-1}) \tag{35}$$

where the vectors $\boldsymbol{r}$ and $\boldsymbol{x}$ respectively collecting all line resistance/reactance parameters.

In addition to the WF network model, one needs to consider the internal WG dynamics due to VAR control loop as simplified by a first-order system (SOENS et al., 2005). The WG's VAR dynamics can be represented by a first-order model, as: (superscript w denoting WG)

$$\Delta\dot{q}^w = -\frac{\Delta q^w}{\tau^w} + \frac{\Delta\hat{q}^w}{\tau^w} \tag{36}$$

where τ^w is the WG's time constant. The equivalent state-space model considering N WGs is:

$$\Delta\dot{\boldsymbol{q}}^w = \boldsymbol{A}^w \cdot \Delta\boldsymbol{q}^w + \boldsymbol{B}^w \cdot \Delta\hat{\boldsymbol{q}}^w \tag{37}$$

with:

$$\boldsymbol{A}^w = \mathrm{diag}(\frac{-1}{\tau_1^w}, ..., \frac{-1}{\tau_N^w}), \text{ and } \boldsymbol{B}^w = \mathrm{diag}(\frac{-1}{\tau_1^w}, ..., \frac{-1}{\tau_N^w})$$

Similarly, the STATCOM's VAR dynamics can be simplified by an equivalent first-order model, as; (superscript s denoting STATCOM)

$$\Delta\dot{q}^s = -\frac{\Delta q^s}{\tau^s} + \frac{\Delta\hat{q}^s}{\tau^s} \tag{38}$$

where τ^s is the STATCOM's time constant. As the STATCOM is typically controlled by a voltage setpoint, the VAR setpoint in (38) is determined by the following s-domain Proportional Integral (PI) control rule:

$$\Delta\hat{q}^s = k^p(\hat{v}^s - v^s) + k^i \int_0^t (\hat{v}^s - v^s)d\tau \tag{39}$$

where k^p and k^i are the fixed gains of the proportional and integral control, respectively.

With the following definition:

$$\Delta v^{int} = \int_0^t (\hat{v}^s - v^s)d\tau \tag{40}$$

where "int"denotes the integration of the deviation $(\hat{v}^s - v^s)$. Combining (33), (38), (39) and (40), one can construct the state space form of the STATCOM as:

$$\begin{bmatrix} \Delta\dot{q}^s \\ \Delta\dot{v}^{int} \end{bmatrix} = \boldsymbol{A}^s \begin{bmatrix} \Delta q^s \\ \Delta v^{int} \end{bmatrix} - \boldsymbol{b}^s\Delta\boldsymbol{q}^w + \boldsymbol{c}^s\Delta\hat{v}^s \tag{41}$$

where matrix $\boldsymbol{A}^s$, and vectors $\boldsymbol{b}^s$, $\boldsymbol{c}^s$ are presented in the Appendix.

The general state space including N^w WGs can be written as:

$$\Delta \dot{\boldsymbol{x}} = \boldsymbol{A}\Delta\boldsymbol{x} + \boldsymbol{B}\Delta\hat{\boldsymbol{u}} \tag{42}$$

where

$$\Delta\boldsymbol{x} = [\Delta q^s, \Delta v^{int}, \Delta q_1^w, ..., \Delta q_N^w]^\top$$

$$\Delta\hat{\boldsymbol{u}} = [\Delta\hat{v}^s, \Delta\hat{q}_1^w, ..., \Delta\hat{q}_N^w]^\top$$

$$\boldsymbol{A} = \begin{bmatrix} \boldsymbol{A}^s & \boldsymbol{b}^s & \dots & 0 \\ 0 & -\frac{1}{\tau_1^w} & \dots & 0 \\ \vdots & \vdots & \ddots & \vdots \\ 0 & 0 & \dots & -\frac{1}{\tau_N^w} \end{bmatrix}$$

$$\boldsymbol{B} = \begin{bmatrix} \boldsymbol{c}^s & \dots & \dots & 0 \\ \vdots & \frac{1}{\tau_1^w} & \dots & 0 \\ \vdots & \vdots & \ddots & \vdots \\ 0 & 0 & \dots & \frac{1}{\tau_N^w} \end{bmatrix}$$

The general state-space model can be discretized to the form $\boldsymbol{x}_{t+1} = \boldsymbol{A}^d\boldsymbol{x}_t + \boldsymbol{B}^d\boldsymbol{u}_t$ to be used as a model prediction, where $\boldsymbol{A}^d$ and $\boldsymbol{B}^d$ are the discrete forms of $\boldsymbol{A}$ and $\boldsymbol{B}$, respectively. The discretized form is done by applying the sampling time $\Delta\tau^p$ using the method described in (TÓTH, 2010).

4.3 Problem formulation

4.3.1 Objective function - Preventive Mode

The preventive mode is switched on when the voltages are within conventional thresholds, and the objective is to set the OC of the WF in such a way that it would have enough reactive power reserve to supply in case of a disturbance.

Proposition 1. *By minimizing the losses in the WF during regular operation, the net VAR used to regulate voltage is minimized, maximizing the VAR reserves in all WGs and STATCOM.*

The ohmic losses can be approximated as a convex quadratic function of power injection by using a second-order Taylor's series expansion over eq. 33 (TAHERI et al., 2020; TURITSYN et al., 2011).

$$L \approx \boldsymbol{p}^T \boldsymbol{R}\boldsymbol{p} + \boldsymbol{q}^T \boldsymbol{R}\boldsymbol{q} \tag{43}$$

Remark 1. *Unlike proposed preventive control such as (ZHAO et al., 2016; ZHAO et al., 2017; GUO et al., 2015) where the objective is to reserve VAR from the STATCOM or CSV, the proposed method in this paper is to "**reserve**"VAR from the whole WF regardless of how much VAR is injected by the STATCOM as long as the WF's net VAR is minimized. This criterion is applied assuming that modern DFIG converters have a time constant similar to the STATCOM.*

Then, for preventive control, the cost function is the voltage deviation from eq.(33) and the losses from eq. (43).

$$
\begin{aligned}
&\boldsymbol{q} = arg \min \left(||\boldsymbol{v} - \boldsymbol{1}||_2^2 + (v_{th} - 1)^2 \right) + \boldsymbol{q}^T \boldsymbol{R} \boldsymbol{q} \\
&\text{s. to:} \\
&\underline{\boldsymbol{q}} \leq \boldsymbol{q} \leq \bar{\boldsymbol{q}} \\
&\boldsymbol{X} \boldsymbol{q} + \boldsymbol{R} \boldsymbol{p} + v_{th} \boldsymbol{1}_N - \bar{\boldsymbol{v}} \leq 0 \\
&- \boldsymbol{X} \boldsymbol{q} - \boldsymbol{R} \boldsymbol{p} - v_{th} \boldsymbol{1}_N + \underline{\boldsymbol{v}} \leq 0
\end{aligned}
\tag{44}
$$

Weights to both parts of the cost function can be applied. After solving the optimization problem; the voltage set-point for the STATCOM can be calculated as:

$$
\hat{v}_s = v_{th} + \boldsymbol{r}_{mv}^T \boldsymbol{p} + \boldsymbol{x}_{mv}^T \boldsymbol{q}
\tag{45}
$$

where $\boldsymbol{r}_{mv}^T := \text{col}_{mv} \boldsymbol{R}^T$ and $\boldsymbol{x}_{mv}^T := \text{col}_{mv} \boldsymbol{X}^T$

The reactive power limits of each WG can be expressed as a function of the terminal voltage and the active power output. Non-controllable buses such as the point of common coupling (PCC), high voltage bus (HV), and medium voltage bus (MV) are also included by setting the constraint $q = 0$. The preventive control is carried out by a centralized controller at the substation. The setpoints are calculated in the range of seconds, which is suitable for a real-time communication system.

4.3.2   Objective function - Corrective Mode

The corrective mode is switched on when the voltages lie out of the thresholds due to a disturbance e.g. an external line transmission fault. The objective is to restore the voltage in all buses once the disturbance is cleared.

Since the centralized controller is sending the set-points within a period of 1 second, a fault can occur at any moment during this period and after the fault is cleared, the last set-points will remain constant until the next set-points are sent by the controller. Because of communication latency restrictions, typically, the voltage is restored by those remaining constant set-points which causes a delayed and undamped voltage recovery (ASADOLLAH; ZHU; LISERRE, 2019).

Nowadays, demanding grid codes require a response time smaller than one second and a maximum overshoot of 5% (MARTÍNEZ et al., 2011).

Remark 2. *Since the time scales during a fault are very short in the range of milliseconds and considering the fast dynamics of the converters, a suitable control time for the transients would be around 50 ms, which is not possible due to communication delays. Therefore, the following formulation is to obtain a training data-set*

The optimization problem aims to restore the voltage within the established thresholds. One can apply a model predictive control (MPC) approach to calculate the control set-points as follows:

$$
\min_{\tilde{q}_q, \tilde{v}_s} \sum_{k=1}^{N_p - 1} \left(||\boldsymbol{v}_{t+1} - \boldsymbol{1}||_2^2 + (v_{th} - 1)^2 \right)
$$

$$
\text{s. to:} \tag{46}
$$

$$
\tilde{\boldsymbol{x}}_{t+1} = \boldsymbol{A}_d \tilde{\boldsymbol{x}}_t + \boldsymbol{B}_d \tilde{\boldsymbol{u}}_t
$$

$$
\underline{\boldsymbol{q}} \leq \boldsymbol{q}_0 + \tilde{\boldsymbol{q}}_{t+1} \leq \bar{\boldsymbol{q}}
$$

Where N_p is the prediction steps and is calculated as $N_p = \frac{T_p}{\Delta T_p}$, being T the prediction time horizon. Such time horizon should be closed to the open-loop settling time of the system (CAMACHO; ALBA, 2013). The sampling time ΔT_p should be smaller than the constant time of the STATCOM.

The constraints regarding voltage thresholds should be relaxed to find feasible solutions since after clearing the fault the voltage will restore from low voltages. In the same way that the preventive mode optimization problem the non-controllable buses are also included by setting the constraint $q = 0$.

The objective of the MPC formulation is to obtain a training data-set for learning purposes to use it in a local fashion. That is the reason why the communication latency is disregarded.

Remark 3

Since the dynamic model is an approximation making some assumptions such as constant active power injection (See appendix), in order to evaluate the performance of the MPC, it should be applied to a system that simulates the real dynamics of the wind generators with a satisfactory degree of fidelity.

4.3.3 Risk-Aware Learning

Recently, decentralized decision rules through supervised learning approaches such as kernel learning and neural networks have been proposed (NNs) (LIU; SHI; ZHU, 2016;

JALALI et al., 2019). Basically, the goal of a machine learning (ML)-based solutions is to obtain the regression model $\Phi(\boldsymbol{y}) \to z$ from the OC y to the optimal z, such that it follows a pre-specified scalable structure. Since our gol is to use local information and any other reachable measurement, one can enforce one model for each WG $\Phi(\cdot)_k, \forall k = 1, ..., N_w$ and for the STATCOM $\Psi(\cdot)_s$.

For each WG we can use the following input features:

$$\boldsymbol{y} = [\hat{q}, q, p, v, p_b]^T \tag{47}$$

where $\hat{q}$ is the actual reactive power set-point, q is the actual reactive power, p is the actual active power, v is the voltage at the WG terminal, and p_b is the total active power of the feeder where the WG is located at.

The input features for the STATCOM:

$$\boldsymbol{y}_s = [\hat{v}_s, q_s, p_{mv}, v_{mv}]^T \tag{48}$$

where $\hat{v}_s$ is the actual voltage set-point, q_s is the actual reactive power injected by the STATCOM, p_{mv} is the total active power at the medium voltage bus, and v_{mv} is the voltage at the medium voltage bus. The output for each WG and the STATCOM are $\hat{z} = \hat{q}$ and $\hat{z}_s = \hat{v}_s$ respectively. Fig.11 shows the schematic learning framework approach for the corrective control.
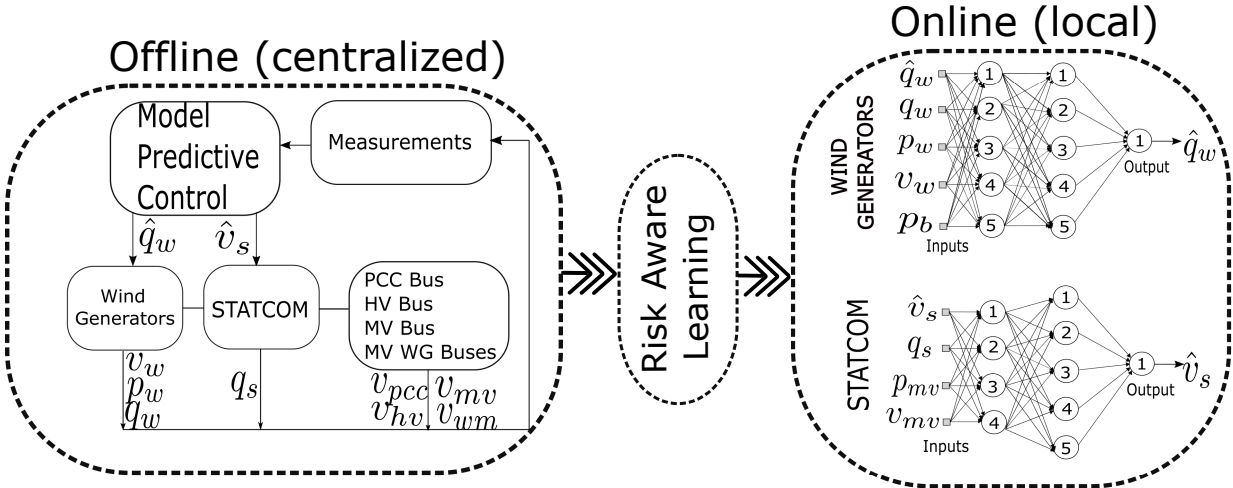
Figure 11 – Learning framework approach for the corrective control.

To develop the mappings $\Phi(\cdot)$ and $\Psi(\cdot)$, a multi-layer perceptron (MLP) Neural Network (NN) can be adopted, well known for being an excellent universal function approximator (LECUN; BENGIO; HINTON, 2015). As an MLP, the architecture of a NN consists of an input layer (features) , hidden layers and output layers (prediction). Each hidden layer consists of n nodes. The output per node n is calculated using the previous layer $\boldsymbol{y}^{l-1}$ as input, where l is the correspondent layer. The previous layer is linearly transformed (using weights and bias) followed by a nonlinear function activation as follows:

$$y_n^{l+1} = \sigma(\boldsymbol{W}_n^l \boldsymbol{y}^l + \boldsymbol{b}_n^l), \quad \forall t = 0, ..., T-1 \tag{49}$$

where $\sigma(\cdot)$ is the nonlinear activation function e.g. ReLU, tanh, sigmoid, etc. The weights $\boldsymbol{W}_n$ and bias b_n are parameters to be learned. From now on, the set of these parameters will be called $\boldsymbol{\varphi}$. $\boldsymbol{\varphi}$ learns through offline training using K data samples. Each sample k contains the input y_k (such as 47 and 48) and the corresponding output z_k. For simplicity, the rest of the thesis will use k to index samples. To train $\boldsymbol{\varphi}$, we aim to minimize the average loss in predicting z over all K samples, as given by:

$$\min_{\boldsymbol{\varphi}} f(\boldsymbol{\varphi}) := \frac{1}{K} \sum_{k=1}^{K} \ell(\Phi(\boldsymbol{y}_k; \boldsymbol{\varphi}), z_k) \tag{50}$$

where $\ell(\cdot)$ denotes the loss function between the predicted and real output value. A commonly used function loss is the L_2-norm called the mean-squared error (MSE). One issue with L_2-norm is that the average loss metric can achieve acceptable values if K is large enough, and predictions with large errors can disguise under apparent a small average loss. These worst-case prediction scenarios can be harmful applied to a voltage control leading to possible voltage overshoots or a slow voltage recovery. To tackle this problem the risk-aware learning approach will be applied, enabling to statistically reduce the risk of prediction with large losses. To quantify the risk of the sample distribution we will use the *conditional value-at-risk* (CVaR), a well known technique used in reinforcement learning problems and robust optimization (GABREL; MURAT; THIELE, 2014; CHOW et al., 2015; CARDOSO; XU, 2019) that has been applied to voltage optimization also (LIN; LIU; ZHU, 2021). To define CVaR we will first pose the α-VaR, where for a given significance level $\alpha \in (0, 1)$, the α-VaR represents the threshold value for the $(1 - \alpha)$-quantile of a random distribution as shown in Figure.12.
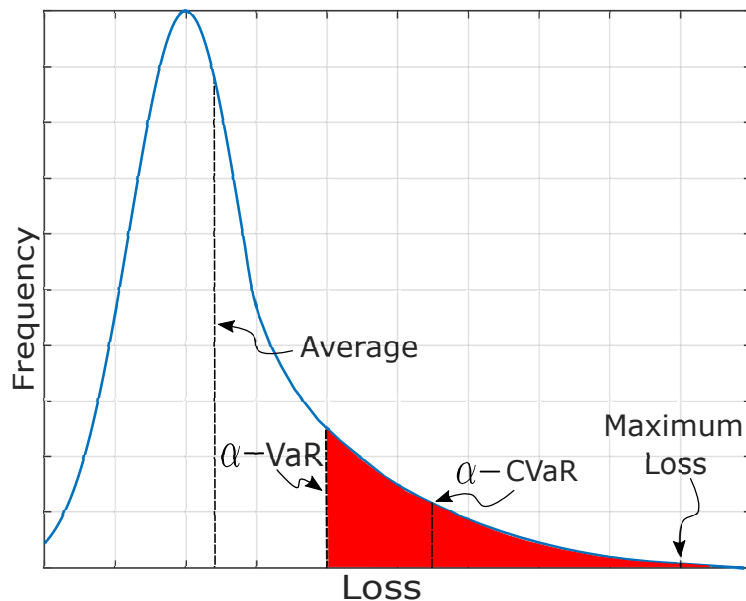

Figure 12 – Comparisson among α-VaR, α-CVaR, and average loss.

Given φ, the α-CVaR is analytically formed by all K samples, as:

$$\gamma_\alpha(\varphi) := \frac{1}{\alpha K} \sum_{k=1}^{K} \ell(\Phi(\boldsymbol{y}_k; \boldsymbol{\varphi}), z_k) \times \mathbb{1}\{\ell(\Phi(\boldsymbol{y}_k; \boldsymbol{\varphi}), z_k) \geq v\} \tag{51}$$

where $\mathbb{1}(\cdot)$ is the indicator function and v is the α-VaR. The CVaR metric can be computed using a bisection typed line search to find v. The corresponding optimization problem can be posed as follows:

$$\gamma_\alpha(\varphi) := \min_{\beta \in \mathbb{R}} \left\{ \beta + \frac{1}{\alpha K} \sum_{k=1}^{K} [\ell(\Phi(\boldsymbol{y}_k; \boldsymbol{\varphi}), z_k) - \beta]_+ \right\} \tag{52}$$

where the positive projection operator $[\cdot]_+ := max\{0, a\}$. The value of β that minimizes (52) is the equal to α-VaR. The advantage and popularity of (52) are due to its convexity property.

4.4 Numerical Validations

The proposed preventive and corrective control is applied to a WF consisting of 20 DFIGs of 3.6 MW divided into 4 feeders of 35 KV. The power is transmitted from the HV/MV substation (115/335) to the PCC through a 115 kV Line 10 km in length. A $\pm$ 20 MVAr Statcom is connected to the MV Bus. The WF is injecting power into the IEEE 9 Bus system. Figure 10 shows the WF configuration.

The MPC was developed in Matlab/Simulink using Yalmix toolbox optimization to solve the quadratic programming problem (LOFBERG, 2004). The WF is created using high fidelity DFIG models in Digsilent PowerFactory software (POWERFACTORY, 2016) that interfaces Matlab to update WG's voltages, active power and reactive power, measurements as a result of the set-points applied.

To create realistic scenarios with a variety of active power injections from each DFIG, one minute of wind field was created using WindSimFarm (GRUNNET et al., 2010) that updates the Wind speed for each feeder considering the wake effect.

4.4.1 Preventive Control Results

The performance of the proposed preventive control is evaluated in two aspects: the loss minimization before the disturbance and its effect on the Critical Clearing Time. For evaluation purposes, we compared the proposed preventive control with another state-of-the-art method in the literature based on DRPR (ZHAO et al., 2016). The simulation starts with different wind speeds for all four feeders changing slowly until a fault causes a disturbance. The initial voltage at the PCC is 1 p.u. Two fault cases are simulated:

❏ **Case 1** : three-phase short-circuit event at Bus 4 cleared after 170 ms.

❏ **Case 2**: three-phase short-circuit event at Bus 7 cleared after 90 ms.

4.4.1.1 Loss minimization performance

The pre-fault condition is the same for all three cases. We can see the proposed preventive control's performance in loss minimization in Figure 13. Compared to the DRPR-based voltage control, the proposed preventive control yields a lower current flowing through the line transmission 3-9 while delivering the same active power. The consequence of this is meaningful since the proposed method provides fewer VAR resources for voltage regulation.
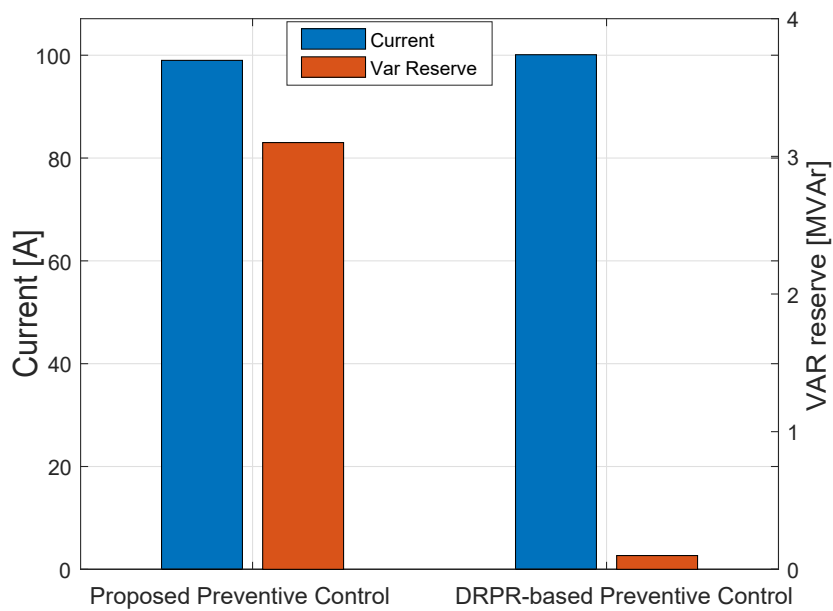
Figure 13 – Comparisson of line transmission (3-9) pre-fault measurements between the proposed and the DRPR based preventive control.

4.4.1.2 Increasing Critical Clearing Time

Despite the preventive control proposed in (ZHAO et al., 2016) yields more DRPR from the STATCOM as shown in Figure 14, the preventive control presented in this paper has better performance regarding voltage restoration and Critical Clearing Times. It can be noticed in Figure 16 that the proposed preventive method yields better voltage restoration even when we use the same corrective control. We can observe in Figure 15 that the system loose voltage stability when applied the DRPR-based preventive control. Table 8 compares the critical clearing time of most representative bus short-circuits between the proposed and the DRPR-based preventive control. In all cases, the proposed preventive control improves the critical clearing time. That means that the loss minimization-based preventive control increases the *Critical Clearing Time.*

Table 8 – Comparisson between critical clearing times between preventive controls

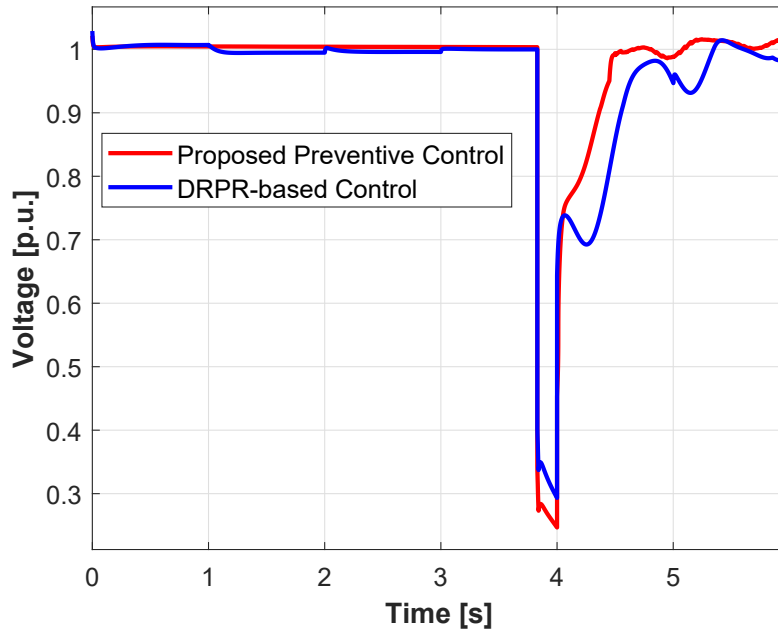|	Critical Clearing Time [ms] (z=0)					
Bus	**4**	**5**	**6**	**7**	**8**	**9**
DRPR-based	170	160	200	90	110	140
Loss Min-based	175	170	220	95	120	155

Figure 14 – Impact of preventive controls on voltage restoration after a fault on bus4.
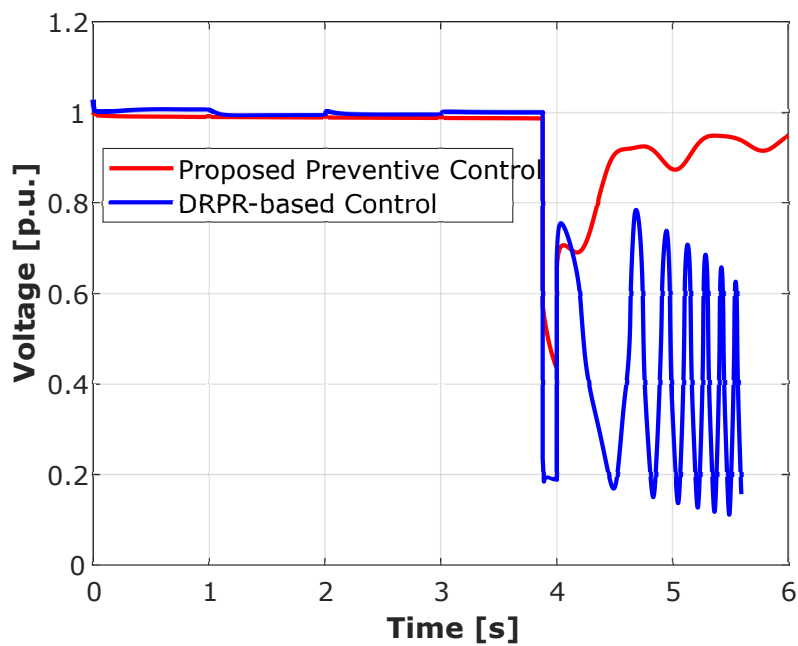

Figure 15 – Impact of preventive controls on voltage restoration after a fault on bus7.

4.4.2   Corrective Control Results

In this section, the performance of the proposed data-driven corrective control is evaluated and compared to the conventional constant set-point applied to the STATCOM and WGs PI controllers, which as stated before uses tha last set-point to restore the voltage.

It is worth nothing that both corrective controls restore the volage trough the STATCOM and WGs PI controllers. The difference lies in the rate of change of the set-point. The data-driven-based control is able to update the set-points every 50 ms for both STATCOM and WGs during the transient, while the conventional control uses the constant pre-fault set-points that only is able to be updated in the range of seconds.

The training data was obtained by simulating faults in all buses in different operating conditions. The set-points for those faults were obtained by performing MPC.The measurements from the fault simulations and their respective set-points from MPC control forms the data-set containing 1055 samples splitted in 80% for training and 20% for testing.

The training process via α-CVaR was implemented using the Pytorch library in Python. Two NN were trained separately, the first one for predicting the STATCOM voltage reference and the second for predicting reactive each WG power injection. After the learning process, the performance of the NNs in the testing data set yielded a maximum prediction error of 7.2% and 8.3% for the STATCOM and WG respectively.

Figures 16 and 17 show the voltage recovery comparison for cases 1 an 2 respectively. For case 2 the fault is cleared before reaching the Critical Clearing Time for the DRPR-based preventive control to prevent voltage collapse. The proposed data-driven corrective control (red line) has a close performance when compared to the idealized MPC control (black line) and for this reason the latest one have been disregarded in the figures.

Since the pre-fault operating condition plays a big role in voltage restoration, the same preventice control has been applied for a fair comparisson. I both cases the proposed data-driven preventive control has better performance than the PI controller with the pre-fault constant set-points.

After the voltage restoration,once the voltage is within the established threshold for one second, the preventive mode is switched on.
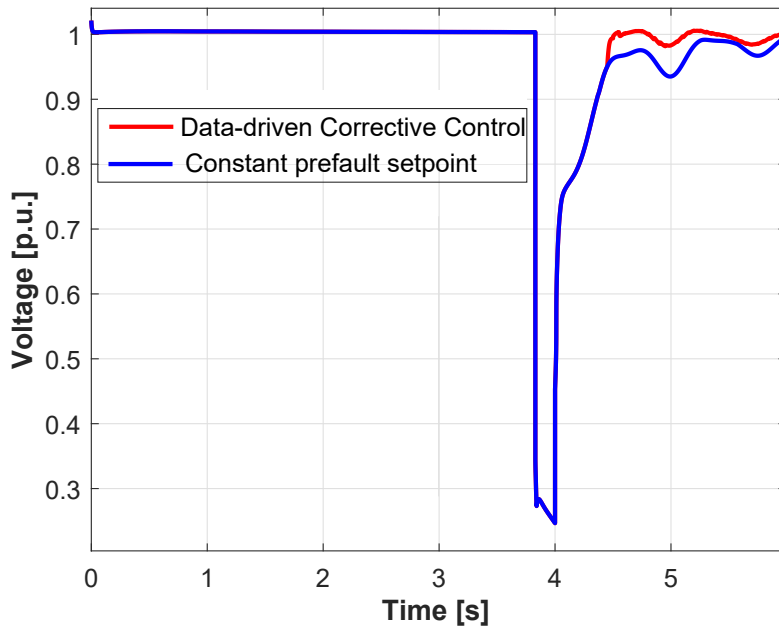
Figure 16 – Voltage at PCC when a fault at bus 4 is applied and cleared after 170 ms; a) Voltage without zoom. b) Zoomed in voltage axis

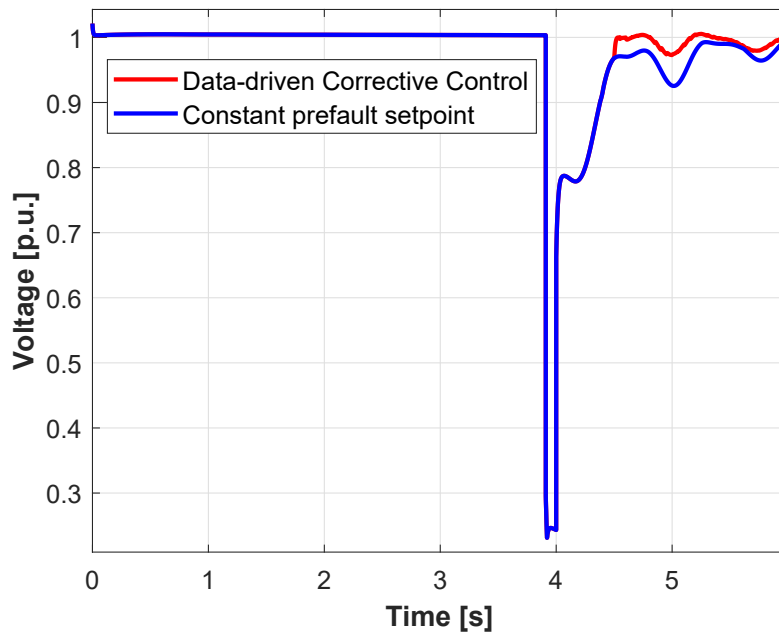Figure 17 – Voltage at PCC when a fault at bus 7 is applied and cleared after 90 ms; a) Voltage without zoom. b) Zoomed in voltage axis

Table 9 shows the comparison of the critical recovering time of most representative buses between corrective controls. In all cases the proposed data-driven control is faster than the conventional one. Again for a fair comparison, the same preventive control is applied before the fault.

Table 9 – Comparisson of critical recovering time between corrective controls

	Critical Recovering Time [sec] (z=0)					
Bus	**4**	**5**	**6**	**7**	**8**	**9**
Constant sp (v=0.9 p.u.)	0.36	0.38	0.365	0.375	0.4	0.41
Constant sp (v=1 p.u.)	$\gg 1$	$\gg 1$	$\gg 1$	$\gg 1$	$\gg 1$	$\gg 1$
Data-driven (v=0.9 p.u.)	0.36	0.38	0.365	0.375	0.39	0.4
Data-driven (v=1 p.u)	0.5	0.52	0.51	0.52	0.55	0.56

4.5   Discussion

While minimizing losses, the proposed preventive voltage control decreases the likelihood of voltage instability by improving critical clearing times and voltage restoration after a disturbance. The proposed data-driven-based corrective voltage control has shown good performance, improving the voltage restoration compared to the conventional pre-fault constant set-points. Due to the efficient *risk aware learning*, the data-driven control can locally set up appropriate set-points, using only local and feeder-head measurements. Due to the low computation time required by the trained neural network, the data-driven corrective control set a new set-point every 0.05 seconds during the transient. As a result, oscillations are also damped, which would not be possible using conventional communication channels.

CHAPTER **5**

Conclusions

This thesis addresses the long and short-term voltage stability, proposing methods to improve real-time monitoring for the first case and to improve voltage restoration and critical clearing times for the latest one. These two aspects of voltage stability play an essential role in the upcoming grids with high penetration of renewable sources to mitigate climate change. The contributions of the thesis for each one of the fields can be highlighted in the following paragraphs.

A new approach to finding saddle-node bifurcation points based on variational theory was presented. One contribution is related to long-term voltage stability. It has been demonstrated that the proposed method can easily track the bifurcation point displaced by a significant disturbance without starting over from the current operating point. The tracking property allows for monitoring the voltage stability margin in real time. It makes the proposed method attractive for finding the bifurcation point of networks with high generation variability, such as those of the upcoming grids with high penetration of renewables.

Another contribution is related to short-term voltage stability. A voltage control that minimizes losses in a wind farm and reduces the possibility of voltage instability during faults was presented. It has been shown that the voltage restoration after a fault does not only depend on the corrective control but also the predictive control. Having an operating condition that minimizes losses before the fault increases the critical clearing time and, consequently, decreases the probability of voltage instability after the fault.

5.1   Published Papers

Salazar, Pablo Daniel Paz and Ilyasov, Yavdat and Alberto, Luís Fernando Costa and Costa, Eduardo Coelho Marques and Salles, Mauricio BC, Saddle-node bifurcations of power systems in the context of variational theory and nonsmooth optimization, IEEE Access,8, 110986–110993, 2020,IEEE.

5.2   Future Work

The future work is related to asses the influence of the wind-farm voltage control over the long-term voltage stability of the system. Also, we aim to use strictly local information for the data-driven control able to achieve good generalization for different operation scenarios.

References

ABBOTT, J. P. et al. Numerical continuation methods for nonlinear equations and bifurcation problems. The Australian National University, 1977.

AJJARAPU, V. Identification of steady-state voltage stability in power systems. **Int. J. Energy Syst.**, v. 11, n. 1, p. 43–46, 1991.

AJJARAPU, V.; CHRISTY, C. The continuation power flow: a tool for steady state voltage stability analysis. **IEEE transactions on Power Systems**, Ieee, v. 7, n. 1, p. 416–423, 1992.

AJJARAPU, V.; LEE, B. Bifurcation theory and its application to nonlinear dynamical phenomena in an electrical power system. **IEEE Transactions on Power Systems**, IEEE, v. 7, n. 1, p. 424–431, 1992.

ALVARADO, F. L. Direct detection of voltage collapse conditions. **Proc. Bulk Power System Voltage Phenomena-Voltage Stability and Security**, p. 523–538, 1989.

ARAPOSTHATIS, A.; SASTRY, S.; VARAIYA, P. Analysis of power-flow equation. **International Journal of Electrical Power & Energy Systems**, Elsevier, v. 3, n. 3, p. 115–126, 1981.

ASADOLLAH, S.; ZHU, R.; LISERRE, M. Analysis of voltage control strategies for wind farms. **IEEE Transactions on Sustainable Energy**, IEEE, v. 11, n. 2, p. 1002–1012, 2019.

AVALOS, R. J. et al. Equivalency of continuation and optimization methods to determine saddle-node and limit-induced bifurcations in power systems. **IEEE Transactions on Circuits and Systems I: Regular Papers**, IEEE, v. 56, n. 1, p. 210–223, 2008.

BAGIROV, A.; KARMITSA, N.; MÄKELÄ, M. M. **Introduction to Nonsmooth Optimization: theory, practice and software**. [S.l.]: Springer, 2014.

BAO, L.; HUANG, Z.; XU, W. Online voltage stability monitoring using var reserves. **IEEE Transactions on Power Systems**, IEEE, v. 18, n. 4, p. 1461–1469, 2003.

BARAN, M. E.; WU, F. F. Network reconfiguration in distribution systems for loss reduction and load balancing. **IEEE Power Engineering Review**, IEEE, v. 9, n. 4, p. 101–102, 1989.

CAMACHO, E. F.; ALBA, C. B. **Model predictive control**. [S.l.]: Springer science & business media, 2013.

CANIZARES, C. A. On bifurcations, voltage collapse and load modeling. **IEEE transactions on power systems**, IEEE, v. 10, n. 1, p. 512–522, 1995.

_____. Applications of optimization to voltage collapse analysis. In: CITESEER. **IEEE-PES Summer Meeting, San Diego, USA**. [S.l.], 1998.

_____. Calculating optimal system parameters to maximize the distance to saddle-node bifurcations. **IEEE Transactions on Circuits and Systems I: Fundamental Theory and Applications**, IEEE, v. 45, n. 3, p. 225–237, 1998.

CANIZARES, C. A.; ALVARADO, F. L. Point of collapse and continuation methods for large ac/dc systems. **IEEE transactions on Power Systems**, IEEE, v. 8, n. 1, p. 1–8, 1993.

CANIZARES, C. A. et al. Point of collapse methods applied to ac/dc power systems. **IEEE transactions on Power Systems**, IEEE, v. 7, n. 2, p. 673–683, 1992.

CARDOSO, A. R.; XU, H. Risk-averse stochastic convex bandit. In: PMLR. **The 22nd International Conference on Artificial Intelligence and Statistics**. [S.l.], 2019. p. 39–47.

CHANDRA, A.; PRADHAN, A. K. Online voltage stability and load margin assessment using wide area measurements. **International Journal of Electrical Power & Energy Systems**, Elsevier, v. 108, p. 392–401, 2019.

CHIANG, H.-D. et al. On voltage collapse in electric power systems. **IEEE Transactions on Power systems**, IEEE, v. 5, n. 2, p. 601–611, 1990.

_____. Cpflow: A practical tool for tracing power system steady-state stationary behavior due to load and generation variations. **IEEE Transactions on Power Systems**, IEEE, v. 10, n. 2, p. 623–634, 1995.

CHOW, Y. et al. Risk-sensitive and robust decision-making: a cvar optimization approach. **Advances in neural information processing systems**, v. 28, 2015.

DEM'YANOV, V. F.; MALOZEMOV, V. **Introduction to minimax**. [S.l.: s.n.].

DEMYANOV, V. F. et al. **Quasidifferentiability and nonsmooth modelling in mechanics, engineering and economics**. [S.l.]: Springer Science & Business Media, 2013. v. 10.

DOBSON, I. Observations on the geometry of saddle node bifurcation and voltage collapse in electrical power systems. **IEEE Transactions on Circuits and Systems I: Fundamental Theory and Applications**, IEEE, v. 39, n. 3, p. 240–243, 1992.

DOBSON, I.; CHIANG, H.-D. Towards a theory of voltage collapse in electric power systems. **Systems & Control Letters**, Elsevier, v. 13, n. 3, p. 253–262, 1989.

DOBSON, I.; LU, L. Voltage collapse precipitated by the immediate change in stability when generator reactive power limits are encountered. **IEEE Transactions on Circuits and Systems I: Fundamental Theory and Applications**, IEEE, v. 39, n. 9, p. 762–766, 1992.

_____. New methods for computing a closest saddle node bifurcation and worst case load power margin for voltage collapse. **IEEE Transactions on Power Systems**, IEEE, v. 8, n. 3, p. 905–913, 1993.

DOEDEL, E.; KELLER, H. B.; KERNEVEZ, J. P. Numerical analysis and control of bifurcation problems (ii): Bifurcation in infinite dimensions. **International Journal of Bifurcation and Chaos**, World Scientific, v. 1, n. 04, p. 745–772, 1991.

ELLIS, A. et al. Reactive power interconnection requirements for pv and wind plants-recommendations to nerc. **Sandia National Laboratories, Albuquerque, New Mexico**, v. 87185, 2012.

GABREL, V.; MURAT, C.; THIELE, A. Recent advances in robust optimization: An overview. **European journal of operational research**, Elsevier, v. 235, n. 3, p. 471–483, 2014.

GÓMEZ-QUILES, C.; GÓMEZ-EXPÓSITO, A.; VARGAS, W. Computation of maximum loading points via the factored load flow. **IEEE Transactions on Power Systems**, IEEE, v. 31, n. 5, p. 4128–4134, 2015.

GRUNNET, J. D. et al. Aeolus toolbox for dynamics wind farm model, simulation and control. In: **The European Wind Energy Conference & Exhibition, EWEC**. [S.l.: s.n.], 2010. v. 2010.

GUO, Q. et al. Hierarchical automatic voltage control for integration of large-scale wind power: Design and implementation. **Electric Power Systems Research**, Elsevier, v. 120, p. 234–241, 2015.

GUO, Y. et al. Enhanced voltage control of vsc-hvdc-connected offshore wind farms based on model predictive control. **IEEE Transactions on Sustainable Energy**, IEEE, v. 9, n. 1, p. 474–487, 2017.

GUTIÉRREZ, R. E. C.; RAMIREZ, J. M. et al. Voltage collapse detection based on local measurements. **Electric Power Systems Research**, Elsevier, v. 107, p. 77–84, 2014.

HAN, T.; CHEN, Y.; MA, J. Multi-objective robust dynamic var planning in power transmission girds for improving short-term voltage stability under uncertainties. **IET Generation, Transmission & Distribution**, IET, v. 12, n. 8, p. 1929–1940, 2018.

HAN, T. et al. Surrogate modeling-based multi-objective dynamic var planning considering short-term voltage stability and transient stability. **IEEE Transactions on Power Systems**, IEEE, v. 33, n. 1, p. 622–633, 2017.

HINGORANI, N. G.; GYUGYI, L.; EL-HAWARY, M. **Understanding FACTS: concepts and technology of flexible AC transmission systems**. [S.l.]: IEEE press New York, 2000. v. 1.

HU, F. et al. Measurement-based real-time voltage stability monitoring for load areas. **IEEE Transactions on Power Systems**, IEEE, v. 31, n. 4, p. 2787–2798, 2015.

IEA. **Global CO2 emissions in 2019**. 2019.

IL'YASOV, Y.; IVANOV, A. Computation of maximal turning points to nonlinear equations by nonsmooth optimization. **Optimization Methods and Software**, Taylor & Francis, v. 31, n. 1, p. 1–23, 2016.

IL'YASOV, Y. S. Bifurcation calculus by the extended functional method. **Functional Analysis and Its Applications**, Springer, v. 41, n. 1, p. 18–30, 2007.

IVANOV, A.; IL'YASOV, Y. S. Finding bifurcations for solutions of nonlinear equations by quadratic programming methods. **Zhurnal Vychislitel'noi Matematiki i Matematicheskoi Fiziki**, Russian Academy of Sciences, Branch of Mathematical Sciences, v. 53, n. 3, p. 350–364, 2013.

JALALI, M. et al. Designing reactive power control rules for smart inverters using support vector machines. **IEEE Transactions on Smart Grid**, IEEE, v. 11, n. 2, p. 1759–1770, 2019.

KELLER, H. B. Numerical solution of bifurcation and nonlinear eigenvalue problems. **Application of bifurcation theory**, Academic, p. 359–384, 1977.

KIWIEL, K. C. **Methods of descent for nondifferentiable optimization**. [S.l.]: Springer, 2006. v. 1133.

KROPOSKI, B. Integrating high levels of variable renewable energy into electric power systems. **Journal of Modern Power Systems and Clean Energy**, SGEPRI, v. 5, n. 6, p. 831–837, 2017.

KUNDUR, P. et al. Definition and classification of power system stability ieee/cigre joint task force on stability terms and definitions. **IEEE transactions on Power Systems**, IEEE, v. 19, n. 3, p. 1387–1401, 2004.

KWATNY, H.; PASRIJA, A.; BAHAR, L. Static bifurcations in electric power networks: Loss of steady-state stability and voltage collapse. **IEEE Transactions on Circuits and Systems**, IEEE, v. 33, n. 10, p. 981–991, 1986.

LECUN, Y.; BENGIO, Y.; HINTON, G. Deep learning. **nature**, Nature Publishing Group, v. 521, n. 7553, p. 436–444, 2015.

LEONARDI, B.; AJJARAPU, V. Development of multilinear regression models for online voltage stability margin estimation. **IEEE Transactions on Power Systems**, IEEE, v. 26, n. 1, p. 374–383, 2010.

_____. An approach for real time voltage stability margin control via reactive power reserve sensitivities. **IEEE transactions on power systems**, IEEE, v. 28, n. 2, p. 615–625, 2012.

LIN, S.; LIU, S.; ZHU, H. Risk-aware learning for scalable voltage optimization in distribution grids. **arXiv preprint arXiv:2110.01490**, 2021.

LIU, H. J.; SHI, W.; ZHU, H. Decentralized dynamic optimization for power network voltage control. **IEEE Transactions on Signal and Information Processing over Networks**, IEEE, v. 3, n. 3, p. 568–579, 2016.

LOFBERG, J. Yalmip: A toolbox for modeling and optimization in matlab. In: IEEE. **2004 IEEE international conference on robotics and automation (IEEE Cat. No. 04CH37508)**. [S.l.], 2004. p. 284–289.

MARTÍNEZ, J. et al. Design and analysis of a slope voltage control for a dfig wind power plant. **IEEE Transactions on Energy Conversion**, IEEE, v. 27, n. 1, p. 11–20, 2011.

MELIOPOULOS, A. S.; COKKINIDES, G.; STEFOPOULOS, G. Voltage stability and voltage recovery: Load dynamics and dynamic var sources. In: IEEE. **2006 IEEE Power Engineering Society General Meeting**. [S.l.], 2006. p. 8–pp.

MILANO, F. An open source power system analysis toolbox. **IEEE Transactions on Power systems**, IEEE, v. 20, n. 3, p. 1199–1206, 2005.

MULLANE, A.; LIGHTBODY, G.; YACAMINI, R. Wind-turbine fault ride-through enhancement. **IEEE Transactions on Power Systems**, IEEE, v. 20, n. 4, p. 1929–1937, 2005.

NEVES, L. S.; ALBERTO, L. F. C.; CHIANG, H.-D. A fast method for detecting limit-induced bifurcation in electric power systems. **Electric Power Systems Research**, Elsevier, v. 180, p. 106101, 2020.

PANNELL, G.; ATKINSON, D. J.; ZAHAWI, B. Minimum-threshold crowbar for a fault-ride-through grid-code-compliant dfig wind turbine. **IEEE Transactions on Energy Conversion**, IEEE, v. 25, n. 3, p. 750–759, 2010.

POWERFACTORY, D. **15, 0 User manual**. [S.l.]: Gommaringen, 2016.

QIAO, W.; HARLEY, R. G.; VENAYAGAMOORTHY, G. K. Coordinated reactive power control of a large wind farm and a statcom using heuristic dynamic programming. **IEEE Transactions on Energy Conversion**, IEEE, v. 24, n. 2, p. 493–503, 2009.

ROCKAFELLAR, R. Directional differentiability of the optimal value function in a nonlinear programming problem. In: **Sensitivity, Stability and Parametric Analysis**. [S.l.]: Springer, 1984. p. 213–226.

ROSEHART, W.; ROMAN, C.; SCHELLENBERG, A. Optimal power flow with complementarity constraints. **IEEE Transactions on Power Systems**, IEEE, v. 20, n. 2, p. 813–822, 2005.

SALLES, M.; FREITAS, W.; MORELATO, A. Comparative analysis between svc and dstatcom devices for improvement of induction generator stability. In: IEEE. **Proceedings of the 12th IEEE Mediterranean Electrotechnical Conference (IEEE Cat. No. 04CH37521)**. [S.l.], 2004. v. 3, p. 1025–1028.

SEYDEL, R. **From equilibrium to chaos**. [S.l.]: Elsevier, 1988.

_____. **Practical bifurcation and stability analysis**. [S.l.]: Springer Science & Business Media, 2009. v. 5.

SOENS, J. et al. Equivalent transfer function for a variable speed wind turbine in power system dynamic simulations. **International Journal of Distributed Energy Resources**, Citeseer, v. 1, n. 2, p. 111–133, 2005.

SUN, H. et al. Review of challenges and research opportunities for voltage control in smart grids. **IEEE Transactions on Power Systems**, IEEE, v. 34, n. 4, p. 2790–2801, 2019.

TAHERI, S. et al. Fast probabilistic hosting capacity analysis for active distribution systems. **IEEE Transactions on Smart Grid**, IEEE, v. 12, n. 3, p. 2000–2012, 2020.

TÓTH, R. **Modeling and identification of linear parameter-varying systems**. [S.l.]: Springer, 2010. v. 403.

TURITSYN, K. et al. Options for control of reactive power by distributed photovoltaic generators. **Proceedings of the IEEE**, IEEE, v. 99, n. 6, p. 1063–1073, 2011.

VIDAL, J. et al. Single-phase dc crowbar topologies for low voltage ride through fulfillment of high-power doubly fed induction generator-based wind turbines. **IEEE Transactions on Energy Conversion**, IEEE, v. 28, n. 3, p. 768–781, 2013.

VOURNAS, C. D.; KARYSTIANOS, M.; MARATOS, N. Bifurcation points and loadability limits as solutions of constrained optimization problems. In: IEEE. **2000 Power Engineering Society Summer Meeting (Cat. No. 00CH37134)**. [S.l.], 2000. v. 3, p. 1883–1888.

VU, K. et al. Use of local measurements to estimate voltage-stability margin. **IEEE Transactions on Power Systems**, IEEE, v. 14, n. 3, p. 1029–1035, 1999.

WANG, Y. et al. Voltage stability monitoring based on the concept of coupled single-port circuit. **IEEE Transactions on Power Systems**, IEEE, v. 26, n. 4, p. 2154–2163, 2011.

YARAMASU, V. et al. High-power wind energy conversion systems: State-of-the-art and emerging technologies. **Proceedings of the IEEE**, IEEE, v. 103, n. 5, p. 740–788, 2015.

YUE, X.; VENKATASUBRAMANIAN, V. M. Complementary limit induced bifurcation theorem and analysis of q limits in power-flow studies. In: IEEE. **2007 iREP Symposium-Bulk Power System Dynamics and Control-VII. Revitalizing Operational Reliability**. [S.l.], 2007. p. 1–8.

ZHAO, H. et al. Coordinated voltage control of a wind farm based on model predictive control. **IEEE Transactions on Sustainable Energy**, IEEE, v. 7, n. 4, p. 1440–1451, 2016.

_____. Combined active and reactive power control of wind farms based on model predictive control. **IEEE Transactions on Energy Conversion**, IEEE, v. 32, n. 3, p. 1177–1187, 2017.

ZHOU, D. Q.; ANNAKKAGE, U. D.; RAJAPAKSE, A. D. Online monitoring of voltage stability margin using an artificial neural network. **IEEE Transactions on Power Systems**, IEEE, v. 25, n. 3, p. 1566–1574, 2010.

ZHOU, L.; SWAIN, A.; UKIL, A. Reinforcement learning controllers for enhancement of low voltage ride through capability in hybrid power systems. **IEEE Transactions on Industrial Informatics**, IEEE, v. 16, n. 8, p. 5023–5031, 2019.

ZHU, H.; LIU, H. J. Fast local voltage control under limited reactive power: Optimality and stability analysis. **IEEE Transactions on Power Systems**, IEEE, v. 31, n. 5, p. 3794–3803, 2015.

Appendix

APPENDIX **A**

STATCOM State Space Model Derivation

Let consider the voltage on the bus (medium voltage) controlled by the STATCOM :

$$v_s = v_{s0} + \tilde{v}_s \tag{53}$$

Since the STATCOM is injecting reactive power to the medium bus voltage, and assuming a constant active power injection during the time horizon:

$$
\begin{aligned}
\hat{v}_s &= (v_{th} + \boldsymbol{r}_{mv}^T \boldsymbol{p} + \boldsymbol{x}_{mv}^T \boldsymbol{q}_f) - (v_{th} + \boldsymbol{r}_{mv}^T \boldsymbol{p} + \boldsymbol{x}_{mv}^T \boldsymbol{q}_0) \\
\hat{v}_s &= \boldsymbol{x}_{mv}^T \hat{\boldsymbol{q}}
\end{aligned}
\tag{54}
$$

Substitute 40 and 54 into 39:

$$\dot{\hat{q}}_s = k_p(\dot{\hat{v}}_s - \boldsymbol{x}_{mv}^T \dot{\hat{\boldsymbol{q}}}) + k_i \dot{\hat{v}}_{int} \tag{55}$$

Substitute 55 into 38:

$$\dot{\tilde{q}}_s = -\frac{\tilde{q}_s}{\tau_s} + \frac{k_p \tilde{v}_s}{\tau_s} - \frac{k_p(\boldsymbol{x}_{mv}^T \tilde{\boldsymbol{q}})}{\tau_s} + \frac{k_i \tilde{v}_{int}}{\tau_s} \tag{56}$$

Substitute 54 and 53 into 40 :

$$\dot{\tilde{v}}_{int} := \dot{\hat{v}}_s - \boldsymbol{x}_{mv}^T \tilde{\boldsymbol{q}} \tag{57}$$

$\boldsymbol{x}_{mv}^T \tilde{\boldsymbol{q}}$ can be decomposed into:

$$\boldsymbol{x}_{mv}^T \tilde{\boldsymbol{q}} = x_{mv-s} \tilde{q}_s + \boldsymbol{x}_{mv-w}^T \tilde{\boldsymbol{q}}_w \tag{58}$$

Equations 56 and 57 form the state space model of the STATCOM:

$$
\begin{bmatrix} \dot{\tilde{q}}_s \\ \dot{\tilde{v}}_{int} \end{bmatrix} = \begin{bmatrix} -\frac{1}{\tau_s}(1 + k_p x_{mv-s}) & \frac{k_i}{\tau_s} \\ -x_{mv-s} & 0 \end{bmatrix} \begin{bmatrix} \tilde{q}_s \\ \tilde{v}_{int} \end{bmatrix} - \begin{bmatrix} \frac{k_p}{\tau_s} \boldsymbol{x}_{mv-w}^T \\ x_{mv-w}^T \end{bmatrix} \tilde{\boldsymbol{q}}_w + \begin{bmatrix} \frac{k_p}{\tau_s} \\ 1 \end{bmatrix} \dot{\hat{v}}_s \tag{59}
$$